56.V

UCRL 3388

UNIVERSITY OF CALIFORNIA

Radiation Laboratory

SOME PROPERTIES OF THE BERYLLIUM NUCLEUS OBTAINED FROM SCATTERING DATA

TWO-WEEK LOAN COPY

This is a Library Circulating Copy which may be borrowed for two weeks. For a personal retention copy, call Tech. Info. Division, Ext. 5545

DISCLAIMER

This document was prepared as an account of work sponsored by the United States Government. While this document is believed to contain correct information, neither the United States Government nor any agency thereof, nor the Regents of the University of California, nor any of their employees, makes any warranty, express or implied, or assumes any legal responsibility for the accuracy, completeness, or usefulness of any information, apparatus, product, or process disclosed, or represents that its use would not infringe privately owned rights. Reference herein to any specific commercial product, process, or service by its trade name, trademark, manufacturer, or otherwise, does not necessarily constitute or imply its endorsement, recommendation, or favoring by the United States Government or any agency thereof, or the Regents of the University of California. The views and opinions of authors expressed herein do not necessarily state or reflect those of the United States Government or any agency thereof or the Regents of the University of California.

UCRL-3388

UNIVERSITY OF CALIFORNIA

Radiation Laboratory
Berkeley, California

Contract No. W-7405-eng-48

SOME PROPERTIES OF THE BERYLLIUM NUCLEUS OBTAINED FROM SCATTERING DATA

Robert G. Summers-Gill

(Thesis)

April 23, 1956

Printed for the U. S. Atomic Energy Commission

SOME PROPERTIES OF THE BERYLLIUM NUCLEUS OBTAINED FROM SCATTERING DATA

Contents

Abstract 3

I. Introduction 5

II. The History of Be^9 7

III. Experimental

A. Introductory Remarks 12

B. The Cyclotron Beam, Scattering Chamber, and Beam Collimation 12

C. The Faraday Cup and Monitoring System, and Measurement of Beam Energy 14

D. The Detector and Associated Electronics 16

E. Targets 20

F. Geometrical Alignment Procedure 21

G. Alignment of Electronics and Use of the Counter . . . 22

H. The Measurement of Differential Cross Sections . . . 29

I. Reduction of Data 30

IV. Results

A. Proton Bombardments 41

B. Alpha-Particle Bombardments 51

C. Deuteron Bombardments 60

V. Discussion 67

A. Elastic Scattering 67

B. The (p, d) Reaction 72

C. The 2.43-Mev State 73

D. Other Levels 81

E. The Three-Body Reactions $Be^9(p, np')Be^8$ and $Be^9(\alpha, n\alpha')Be^8$ 84

F. Remarks About the Direct Interaction Theories . . . 87

VI. Conclusions 90

Acknowledgments 91

Appendix 92

References 96

SOME PROPERTIES OF THE BERYLLIUM NUCLEUS OBTAINED FROM SCATTERING DATA

Robert G. Summers-Gill

Radiation Laboratory
University of California
Berkeley, California

April 23, 1956

ABSTRACT

A beryllium target has been bombarded with 12-Mev protons, 24-Mev deuterons, and 48-Mev alpha particles. With the three projectiles the differential cross sections for inelastic scattering leading to the formation of the 2.43-Mev state have been measured. Application of inelastic scattering theory leads to the assignment 5/2 and odd parity for this level.

A very weak inelastic proton group has been found, confirming the recently reported "level" in Be^9 at ~1.8 Mev. It is pointed out, however, that the observations can also be explained on the basis of heavy-particle stripping in the reaction Be^9 (p, np') Be^8. The observation of inelastic alpha-particle groups corresponding to levels at 6.8 and 11.3 Mev permits the assignment of isotopic spin 1/2 to these states. The data obtained were not inconsistent with the existence of levels at 3.1 and 4.8 Mev.

The pickup reaction Be^9 (p, d) Be^8, in which Be^8 is left in its ground state, was also observed. While the distribution of deuterons is peaked forward as predicted by Butler stripping, its shape is the same as that found at other energies. Such behavior is not in agreement with the quantitative aspects of the theory.

The reactions Be^9 (p, np') Be^8 and Be^9 (α, nα') Be^8 have been studied. Analysis of the angular distributions suggests that those processes in which the charged particle retains most of the energy occur predominantly by direct interaction.

Finally, the elastic scattering of protons, deuterons, and alpha particles has been observed. Analysis of the distributions on the basis of a black nucleus gives reasonable agreement with the positions of the diffraction features. The radii of interaction necessary are large, but consistent within themselves and with those which fit the inelastic data.

I. INTRODUCTION

The basic problem of nuclear physics is to discover the laws that govern the forces between nucleons. Unfortunately there are no single experiments that can give this information in its entirety. There seem to be two approaches that yield certain of these properties. One is the investigation of single nucleons and their relationship to the mesons which are quanta of the force field. The second is the investigation of nuclear structures, the entities that these forces bind together. It is the latter approach with which this discussion is concerned.

A nucleus generally has a ground state which may or may not be stable and many quasi-stable excited states or levels. These are characterized by the quantum mechanical properties, excitation energy, angular momentum or spin, parity, and isotopic spin. The last-mentioned has validity only in the region of the light nuclei, where $N \approx Z$. In addition, there are any number of secondary quantities--such as the electric and magnetic multipole moments, mode of decay, formation cross section, lifetime, nuclear radius, etc.--that provide additional criteria for the selection of a correct nuclear model. It is the job of the experimentalist to determine such information and to make comparisons with the predictions of theory.

A nuclear reaction can, in general, be written

$$A + X \rightarrow B + Y,$$

where A is the target nucleus, X the bombarding particle, B the residual nucleus, and Y the outgoing particle. The discussion has been limited to two-body processes only. If the particle X has a single energy E_x, then the particles Y will be observed with a set of energies E_{yi}, where

$$E_{yi} = E_x + Q - E_{Bi} .$$

The term Q is the usual energy release of a nuclear reaction, and is related to the ground-state masses of the nuclei involved; E_{Bi} is the

excitation energy of the i-th level of the nucleus B. In the light nuclei, where the excited states are widely separated, the discrete values of E_{yi} manifest themselves in easily resolvable particle groups of different energies. The angular distribution of the outgoing particles is determined by the spins and parities of the initial and final nuclei and by the reaction mechanism. As a consequence, the measurement of such angular distributions can yield information about the properties of the energy levels involved.

It is beyond the scope of this discussion to follow these general ideas further. In particular, one reaction of this type for which the reaction mechanism is fairly well understood is inelastic scattering. In such a reaction the particles X and Y are the same, so that the nuclei A and B differ only in that while A is necessarily in its ground state B may be left in any of its characteristic levels. In an effort to determine the properties of the excited states of Be^9 an investigation of reactions of this type was undertaken that used the protons, deuterons, and alpha particles available at the 60-inch cyclotron. (The methods of analysis of these studies are described in detail as they are encountered.) In the course of this work other related reactions involving Be^9 as the initial nucleus were also studied.

II. THE HISTORY OF BERYLLIUM-9

Although the beryllium nucleus was early the subject of considerable experimental investigation, its energy-level structure is poorly and incompletely determined. This is perhaps due to its very low neutron binding energy, 1.666 Mev. As a consequence, nuclear reactions involving Be^9 are generally accompanied by a considerable amount of multibody breakup, for the escape of a neutron leads to the formation of alpha-unstable Be^8.

Because of uncertainty in the type of nuclear model applicable, theoretical understanding has been slow also. On the one hand, the alpha-particle model[1] has exhibited considerable success in explaining the behavior of Be^8. Treatment of the loosely bound neutron as a perturbation to the alpha-particle model[1] is therefore possible. On the other hand, the wider applicability of the shell model is attractive. In the j-j coupling limit,[2] the properties of the lower-lying levels of Be^9 should be due to the single odd neutron. Recent extensions of the shell model to intermediate coupling[3] appear to be more realistic, but unfortunately require lengthy numerical computations. The most recent nuclear model,[4] in which collective modes are considered, is being applied to the Be^9 data in an attempt to obtain a better understanding. That work, however, is unpublished, so that it is impossible to judge its merits at present. Throughout these analyses, the theorist is hampered by the paucity of experimental evidence.

Shown in Fig. 1 is the presently known energy-level diagram of Be^9. For a complete listing of the experiments on which this is based the reader is referred to the excellent review article[5] from which this diagram was taken and to the earlier reviews in the same series. A brief summary of the existing information follows.

(a) <u>The ground state</u>. As is usually the case, the ground-state properties are the most extensively known. The spin is 3/2, the parity is odd, and the magnetic moment is -1.178 nuclear magnetons. The mirror nucleus B^9 is unstable and decays into Be^8 plus a proton.

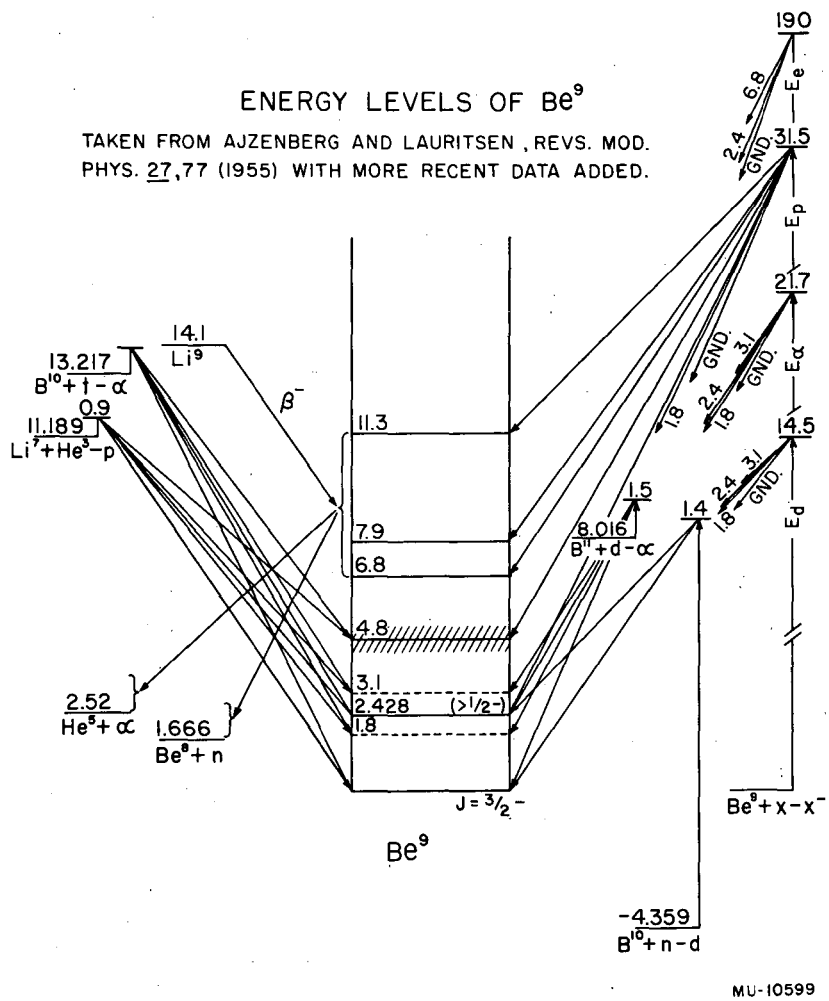

Fig. 1. Energy levels of Be^9. (Taken from Ajzenberg and Lauritsen, Revs. Modern Phys. 27, 77 (1955), with more recent data added.)

(b) Neutron threshold. The threshold for neutron emission is 1.666 Mev. Thus the neutron is bound with less energy than in any other stable nucleus.

(c) The 1.8-Mev state. An $s_{1/2}$ level at about this excitation was predicted by Guth[6] on a single-particle model to explain the behavior of the (γ, n) cross section near threshold. No further evidence for a level at this excitation was found until Moak, Good, and Kunz[7] reported the results of a study of the reaction $Li^7(He^3, p)Be^9$ at 720 kev laboratory energy. Although three-body breakup was present, a peak corresponding to a level at 1.8 Mev was prominent. In order to confirm its presence, Lee and Inglis[8] repeated earlier work on the magnetic analysis of the reaction $B^{11}(d, \alpha)Be^9$. A very weak indication of this level was reported. When the experiments described herein were undertaken, this level had not been detected in inelastic scattering experiments. Recently, however, groups at Rice[9] and Indiana[10] have observed weak indications of inelastic particle groups which could correspond to a level at this excitation. Considerable doubt exists, however, whether the effects seen are due to a level in Be^9 or whether they are merely manifestations of resonance properties of the unbound $Be^8 + n$ system. Careful investigation[11] of reactions leading to B^9, the mirror nucleus, fail to show any clear indication of a level in the vicinity of this energy of excitation.

(d) The 2.43-Mev state. This level has been observed in many experiments, namely

$Be^9(e, e')Be^{9*}$ at 190 Mev;[12]
$Be^9(p, p')Be^{9*}$ at 5.2 Mev,[9]
7.1 Mev,[13]
7.5 Mev,[14]
31.3 Mev;[15, 16]
$Be^9(d, d')Be^{9*}$ at 10.8 Mev,[10]
14.5 Mev;[17]
$Be^9(\alpha, \alpha')Be^{9*}$ at 21.7 Mev;[18]
$Be^{11}(d, \alpha)Be^{9*}$ at 1.51 Mev;[19]
$Be^{10}(n, d)Be^{9*}$ at [illegible]14 Mev;[20]
$Be^{10}(t, \alpha)Be^{9*}$ at low energy;[21]
$Li^7(He^3, p)Be^{9*}$ at 720 kev,[7]
900 kev.[22]

Unfortunately, most of these measurements have been carried out at only one angle and lack absolute normalization, so that little information about the cross section for formation is known. The most precise magnetic spectrometer measurements lead to an excitation energy of 2.428 ± 0.003 Mev. The level is reported to have a natural width less than 3 kev.[23] Dissanaike and Newton[24] found that it decays predominantly by neutron emission to the ground state of Be^8. In an inverse Butler[25] stripping reaction Ribe and Seagrave[20] concluded that the level has odd parity and $3/2 \leq J \leq 9/2$, the same result as they obtained for the Be^9 ground state. A comparison of the inelastic proton data at 31 Mev with the theory of Austern, Butler, and McManus[26] (hereinafter referred to as the ABM theory) led Finke[16] to assign the level even parity and $1/2 \leq J \leq 7/2$.†

(e) The 3.1-Mev state. Like the 1.8-Mev level, this was first discovered in the reactions $Li^7(He^3, p)Be^{9*}$[7] and $B^{10}(t, \alpha)Be^{9*}$.[21] More recently the experiments by Lee and Inglis[8] and by Rasmussen et al.[10] have shown that this level is weakly excited in other reactions.

(f) The 4.8-Mev state. This state, which appears to be broad, has been observed by Moak et al.[7] and Benveniste et al.,[16] and in the reaction $B^{10}(t, \alpha)Be^{9*}$.[21]

(g) The states at 6.8, 7.9, and 11.3 Mev. For the most part experimenters have not had sufficient energy to produce these states. The presence of these states has been established by inelastic proton scattering.[16] The 6.8-Mev level has also been observed in inelastic electron scattering at 190 Mev.[12] Rough data[27] indicate that Li^9 decays by β^- emission to these highly excited states of Be^9 (or other states in the same region). No precise information about the end-point energy or the complexity of the decay scheme is available, however.

(h) States with energies above the proton threshold. The proton threshold in Be^9 is 16.871 Mev. In the region 17 to 22 Mev many levels have been observed in 31-Mev proton bombardment[16] and inferred from

†In a recent article based on this work the authors re-examine the data and suggest that J=1/2, 3/2, 7/2, or 9/2 and odd parity is a possibility.

the behavior of yield measurements[28] of the reactions $Li^7(d,n)Be^8$ and $Li^7(d,p)Li^8$. These levels are too high in excitation and too closely spaced to permit investigation in the work reported herein. For the same reasons their interpretation with present nuclear models is impossible.

In addition to the above level data, the energy dependence of the photonuclear reactions $Be^9(\gamma,n)Be^8$[29] and $Be^9(\gamma,p)Li^8$[30] has been measured. Comparison of these cross sections led Nathans and Halpern to suggest that the alpha-particle model was applicable.

The experiments described in this paper were carried out with four major goals in mind:

1. A detailed examination of the 1.8-Mev level, in order to verify its existence and to determine the cross section for its formation. If possible, angular-distribution measurements were planned to permit evaluation of the spin and parity involved.

2. Determination of the cross sections for the formation of the 2.43-Mev state in order to resolve the disagreement in parity mentioned above. Further, it was hoped that an unambiguous spin assignment might be made possible by combining proton, deuteron, and alpha-particle data.

3. Examination of as many of the more excited states as reaction kinetics permitted. Cross-section measurements, if possible, would allow spin and parity assignments. Moreover, presence or absence of these levels in alpha-particle excitation would permit isotopic-spin assignments.

4. Measurement of elastic scattering cross sections for the determination of the nuclear radius from optical model considerations. In particular, in such a loosely bound structure one might expect a conspicuous deviation from the usual $r_0 A^{1/3}$ law.

As will be seen in what follows, these aims could not be completely fulfilled. This was due in part to the smallness of the cross sections for the formation of some of the excited states. The major experimental difficulty, however, was the dominating presence of charged particles from multibody reactions.

III. EXPERIMENTAL

A. Introductory Remarks

In order to determine differential scattering cross sections with the formation of specific excited states, four items are required: (a) an incident beam of particles, (b) a target, (c) a device for measuring the amount of incident beam, and (d) a detector of the scattered particles. To obtain the required angle and energy resolution the incident beam must be reasonably momoenergetic and parallel, the target must be thin, and the counter must subtend a sufficiently small angle and provide energy selection. The manner in which these criteria were satisfied is described in the following subsections. Descriptions of the equipment itself are, for the most part, brief, since accounts have already been published by Fischer,[31] Ellis,[32] and Vaughn.[33] However, since the problems encountered in this work were somewhat different from those in the foregoing experiments, the methods followed are discussed in more detail.

B. The Cyclotron Beam, Scattering Chamber, and Beam Collimation

The external beam of the 60-inch cyclotron at Crocker Laboratory was used. This accelerator produces beams of 12-Mev protons, 24-Mev deuterons, and 48-Mev alpha particles. Figure 2 is a simplified schematic diagram of the experimental arrangement. The particle beam, extracted by the electrostatic deflector, passed through the cyclotron fringing field via the iron snouts shown. It was then strong-focused by the two-unit quadrupole lens and led the 12 feet through the water shielding to the 36-inch scattering chamber in a 2-inch-diameter brass pipe. The aperture of the lens system was determined by the adjustable slit immediately in front of the strong-focusing magnets.

The scattering chamber was designed to permit as much remote operation as possible to avoid interruption in cyclotron operation during the course of the experiments. The detector was mounted on a table which could be rotated to position the former at any desired angle

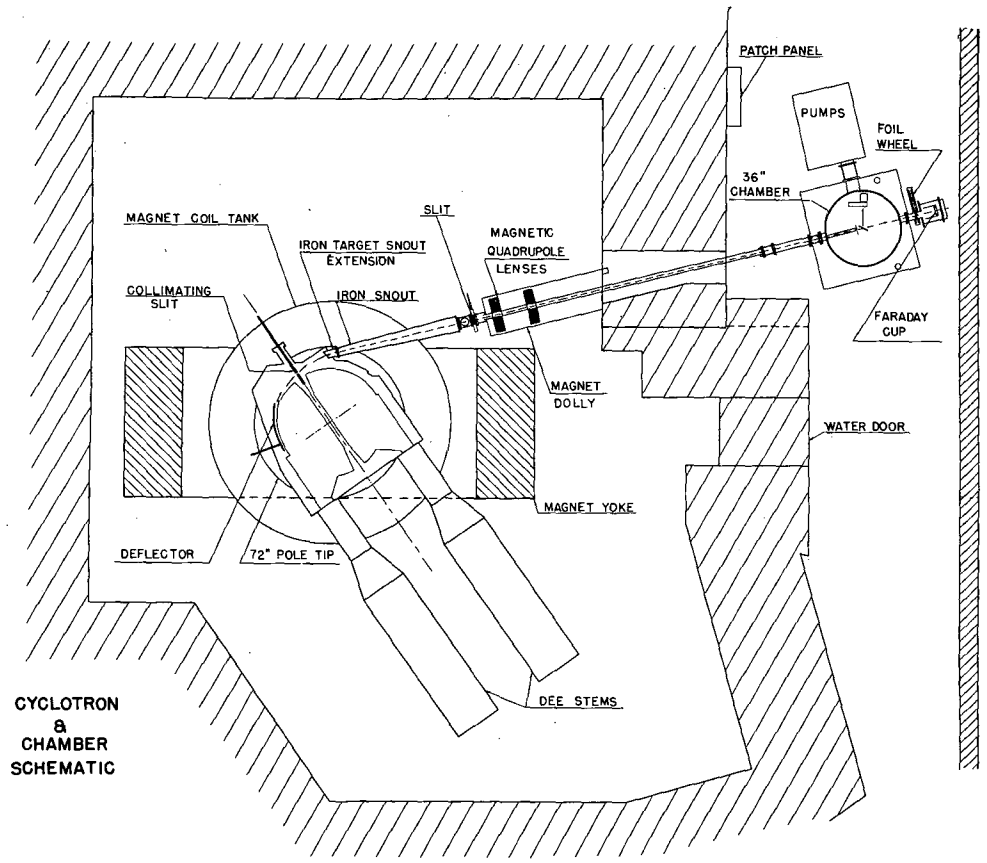

Fig. 2. Schematic diagram of the cyclotron and scattering chamber

to the beam direction. The target, mounted from the lid of the chamber, could also be rotated to any desired orientation. In addition, to permit removal and change of targets during operation, the target assembly could be raised and lowered. All these movements were made by remote control; the positioning was communicated to the counting area by means of micro switches and selsyn repeater systems. An aperture at the rear of the scattering chamber allowed the beam to enter a Faraday cup behind.

It has already been mentioned that partial beam collimation was achieved through the use of the lens aperture slit and the strong-focusing system. In addition, three circular carbon collimators (the smallest with a 1/8-inch-diameter hole) could be positioned either in the brass pipe just outside the chamber or inside the scattering chamber itself, so that the nearest was only some 3 inches from the target. Three different collimation arrangements were thus available: circular collimators inside the chamber, circular collimators outside the chamber, or no circular collimators at all. With each arrangement the beam spot at the target position was about 1/8 inch in diameter. To minimize counter background each arrangement had its application during the course of these experiments.

The maximum beam current available in this way was usually more than enough to give satisfactory counting rates in the detector. General operating beams ranged from 10^{-4} to 10^{-1} microampere depending on the magnitude of the scattering cross section being measured.

C. The Faraday Cup and Monitoring System, and Measurement of Beam Energy

As mentioned, a Faraday cup was attached at the rear of the scattering chamber. The beam charge collected on this was integrated on capacitors of known value. The resultant voltage was measured by a standard Radiation Laboratory negative-feedback electrometer and displayed on a Speedomax Recorder. After collection of predetermined amounts of charge the scaling equipment was automatically gated off to await recording of the data.

A thin NaI crystal and its viewing photomultiplier were placed outside the chamber at 20° to the incident beam direction. Particles scattered at this angle from the target were admitted to this monitor through a thin aluminum window. After amplification and discrimination the output pulses from the phototube were fed to a counting-rate meter in the cyclotron control room to provide the operators with a continuous indication of the beam intensity. The same output was also fed in parallel to a scaler in the counting area. Since the crystal remained at a constant fixed angle, for a given scattering target the number of monitor counts was directly proportional to the number of incident particles. After calibration against the Faraday cup, this crystal arrangement served as a secondary beam-measuring device. It therefore provided a check on the correct operation of the Faraday cup during runs.

Its counting rate also provided the only beam-intensity measurement when data were being taken at extreme forward scattering angles. This was because the outer case of the detector obscured the Faraday cup aperture when the counter was positioned at angles less than 7°.

Beam-energy measurements were carried out by determining the range in aluminum of the incident beam. Immediately in front of the Faraday cup were two remotely controlled wheels, each holding ten aluminum absorbers, plus two blanks to permit normal integration of the incident beam. One of these, the so-called "thick wheel," was rotated until the thickest foil, which did not reduce the amount of beam transmitted, was positioned over the entrance to the Faraday cup. Then, by rotating the "thin wheel," one could obtain a plot of the beam intensity versus absorber. Analysis of an integral range curve of this type yields the mean energy and the beam resolution. From several determinations the latter was found to be approximately 1%. Although the mean energy was observed to be a function of cyclotron operating parameters, particularly deflector voltage and oscillator power, its variation from run to run was never more than 1%. Allowing for the 1.5% energy loss in the beryllium target used in these experiments, best values for the energies in the target were:

protons	12.0 ± 0.2 Mev,
deuterons	24.0 ± 0.4 Mev,
alpha particles	48.0 ± 0.9 Mev.

D. The Detector and Associated Electronics

As already mentioned, to be useful in an experiment of this type, the detector must have adequate angle and energy resolution. Acceptance angle can be made as small as desired by using a suitably small entrance aperture. In this particular case, since the angular spread of the incident beam was of the order of 1°, nothing was to be gained by going to better resolution than this. The aperture used was 0.25 in. in diameter at a distance of 12 in. from the target. For measurements at small scattering angles, in order to reduce the detector sensitivity and so avoid the necessity of operating the cyclotron at micromicroampere beam levels, a second aperture 1/40 as large as the first was available. This could be moved in and out of position by remote control.

Energy resolution was achieved by using a three-chamber proportional counter telescope and variable aluminum absorbers. Complete details of the counter assembly are given by the designer.[32] A schematic is shown in Fig. 3. Particles of the desired energy were detected by interposing an appropriate amount of absorber so that they came to rest somewhere in the interval between just entering the second chamber and just entering the third. The second and third chambers were thus used in anticoincidence. The first chamber, in coincidence with the second, provided a counter telescope and pulse-height discrimination. The effective thickness of the counter from front to range foil (the foil separating Chambers 2 and 3) was about 19 mg/cm^2 of aluminum. Consequently a low-energy detection cutoff existed--3.0 Mev for protons, 3.6 Mev for deuterons, and 12 Mev for alpha particles. The flatness of the range-energy dependence at low energy imposes a resolution cutoff too. The latter proves to be more of a limitation.

Figure 4 shows a block diagram of the counter electronics as well as the circuitry used in connection with the monitor and Faraday cup already described. Separate positive high voltage (not shown) was

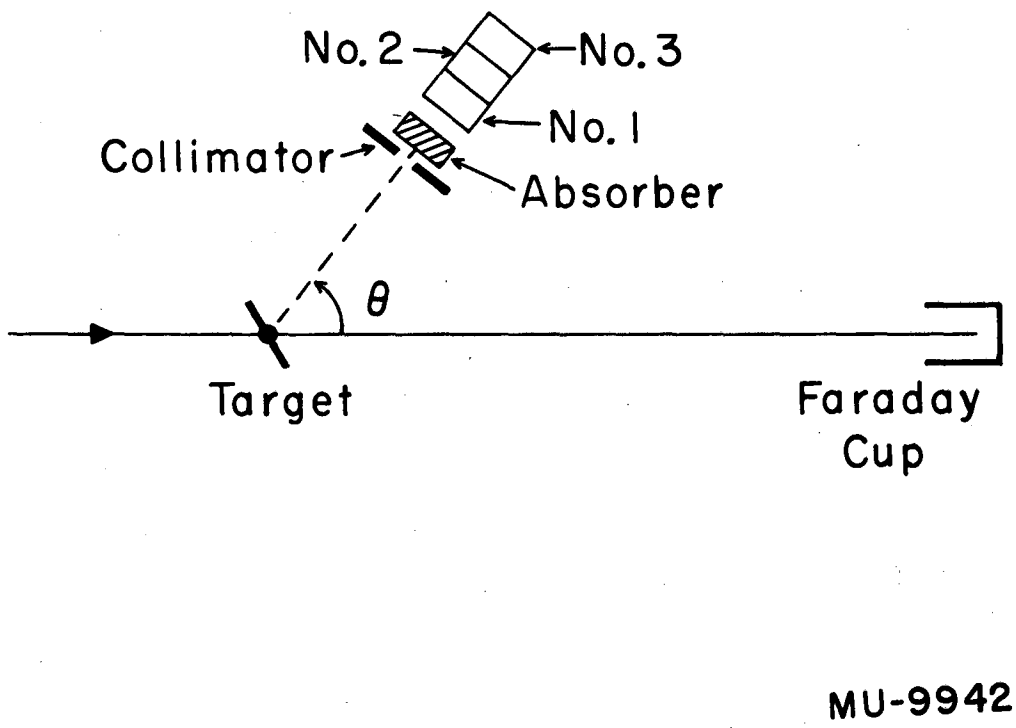

Fig. 3. Schematic diagram of the detector.

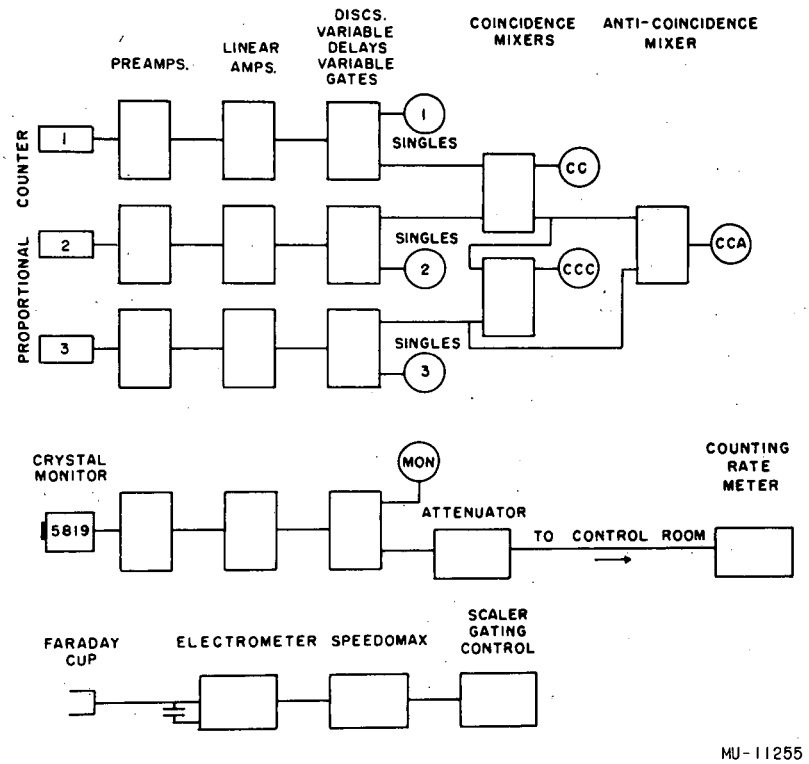

Fig. 4. Block diagram of the electronics.

supplied to each chamber of the detector. By means of a precision resistance chain and a Leeds and Northrup potentiometer, voltages could be set and measured to 1 part in 2500. During runs lasting more than a week no drifts of more than 2 volts in 1500 were ever observed. Counter pulses were delay-line clipped to 1 microsecond duration and fed to preamplifier circuits near the scattering chamber. These provided 75x amplification, with cathode-follower output matched to the coaxial line. After reaching the counting area, the pulses were fed to linear amplifiers whose outputs were coupled to standard variable-delay variable-gate discriminator circuits. The output gate pulses were mixed in the desired manner in 8-channel quadruple-coincidence circuits. The timing of the gate pulses was carefully checked on an oscilloscope at frequent intervals during the runs. Since all circuits were on stabilized power and were thermostatically maintained at constant temperature, few drifts occurred. With these coincidence networks three types of events were recorded--those corresponding to the passage of a particle through Chambers 1 and 2, those corresponding to the passage of a particle through all three chambers, and those in which Chambers 1 and 2 were triggered while the third was not. These will be referred to as CC's, CCC's, and CCA's respectively. It will at once be appreciated that CCA = CC - CCC. Close agreement between the CCA and the subtraction provided assurance that the system was operating properly. Because anticoincidence circuits are less trustworthy the subtraction was considered the more accurate. The singles in each of the counters were recorded to permit check of the individual counting rates. In order to determine that accidental coincidences were few in number it was only necessary to introduce extra delay into any of the three gate-producing circuits.

The variable aluminum absorber consisted of 11 foils between the entrance aperture and the counter. These could be interposed or withdrawn individually by means of solenoids operated from the counting area. The smallest of these foils was 0.601 mg/cm^2, the others being twice, four times, eight times, etc., as thick. In this way the total amount of absorber could be varied from 0.60 to 1230 mg/cm^2 in steps of 0.60 mg/cm^2. A twelfth solenoid controlled the smaller entrance aperture

mentioned above. The foils and the sensitive volume of the counter were sufficiently large in area so that only a negligible fraction of the particles passing through the aperture would escape detection because of multiple scattering in the absorber.

E. Targets

All of this work was done using the same 1-mil beryllium target. Its size, 1.5 by 1 in., permitted the supporting brass frame to be well removed from the incident beam. Its exact thickness was determined by weighing the careful measurement of its area with a traveling microscope. The value obtained checked with a measurement of the beam energy loss in the target. As mentioned above, this energy loss introduced only a 1.5% uncertainty in the reaction energy. The root-mean-square multiple-scattering angle for all beams was less than 1°. Only a negligible amount of the transmitted beam, therefore, escaped detection in the Faraday cup. The purity of the target was checked by spectroscopic analysis. Only trace amounts of Mg, Ca, and Fe were found. There was a larger amount of oxygen contamination, however. This manifested itself in the presence of elastically scattered particle groups (shown in Fig. 9 for protons) whose energies were characteristic of a mass-16 recoil. From the ratio of the intensities of the oxygen and beryllium elastic proton groups at 90° and the cross section for O^{16} (p, p) O^{16}(measured[34] at 19 Mev and corrected for a $1/E^2$ dependence and diffraction effects to 12 Mev), this oxygen content was found to be less than 1%.

In order to permit alignment of the counter electronics with more nearly monoenergetic scattered particles, a thin gold target was provided also.

F. Geometrical Alignment Procedure

Scattering runs were usually of 6 days' duration. Geometrical set-up, in which every precaution was taken to insure that the beam traversed the scattering chamber in the correct manner, generally was completed in 12 hours. Alignment was begun by taking nuclear emulsion pictures of the beam at the end of the long iron snout. At this point the beam was rectangular in cross section with its longest dimension in the horizontal plane. By adjustment of the orientation of the snout and by the addition of extra iron for more effective magnetic shielding the "hot spot" was centered in the aperture. The lens aperture slit and the 12-foot brass beam duct were then attached and further pictures taken at the far end to locate the normal beam trajectory. Under these conditions, the beam was very diffuse and filled the aperture of the pipe. After satisfactory crude alignment, the strong-focusing magnets were energized. Adjustment of their positioning and strength was continued until pictures showed a nearly clean round spot about 1/8 in. in diameter.

At this stage the scattering chamber was moved into approximate position and alignment continued visually by means of a telescope mounted at the Faraday cup aperture. As a final check further beam patterns were taken in the plane of the target position. The strong-focusing magnet current was generally reduced about 10% to provide optimum focus at this greater distance. A final check of the alignment of the carbon collimators (in the desired position of installation) and of the detector and target remote position indicators completed geometrical alignment.

Not previously mentioned but also fastened to the movable table within the scattering chamber was a metal plate in which a 1/16-in.-wide vertical slot had been cut. Mounted 45° counterclockwise from the detector, it permitted the measurement of the beam profile. With the target in position this slot was moved across the front of the Faraday cup aperture in 0.25° intervals. At each setting the cup current corresponding to a suitable constant number of monitor counts was recorded. Since the monitor counts were proportional to the beam incident on the target and hence entering the chamber, and as the Faraday cup measured

the beam passing through the slot, a beam profile was obtained. Typical profiles are shown in Figs. 5a, 5b, and 5c for the various positions of the carbon collimators used in the proton, deuteron, and alpha-particle bombardments. In spite of the care with which geometrical alignment was made, the centers of these distributions generally deviated from the 0° axis of the chamber by 0.2° or 0.3°. These deviations were noted and the laboratory angles of all measurements corrected accordingly.

G. Alignment of Electronics and Use of the Counter

All adjustments were carried out with the gold target in position and the counter set at some convenient forward angle, 25° for example. Since elastic scattering predominates under these conditions, an essentially monoenergetic beam was available. The counter could not be placed in the direct beam itself, since even the smallest beam level was too intense.

For alpha particles, counter high voltages were generally set near 1350 volts; for protons and deuterons voltages closer to 1450 were common. The three gate pulses were brought into time coincidence with the variable delays and adjusted in length so that those from Chambers 1 and 2 were 1 microsecond in duration and those from Chamber 3 were 2 μsec. With sufficient absorber in front of the counter so that the particles were stopping in Chamber 1, the first linear amplifier was adjusted so that the mean output pulse height was approximately 50 volts. The absorber was reduced to allow the particles to stop in the second chamber, and the second linear amplifier adjusted in the same way. Similarly the third linear amplifier was adjusted. This process insured that the pulses from each chamber were being amplified to about the same extent and further that the maximum possible pulse size would never cause overloading.

Most often the counter was used differentially, that is, it was used to detect particles whose ranges lay in the interval R to $R + \Delta R$. The discriminators were set to achieve that result as follows.

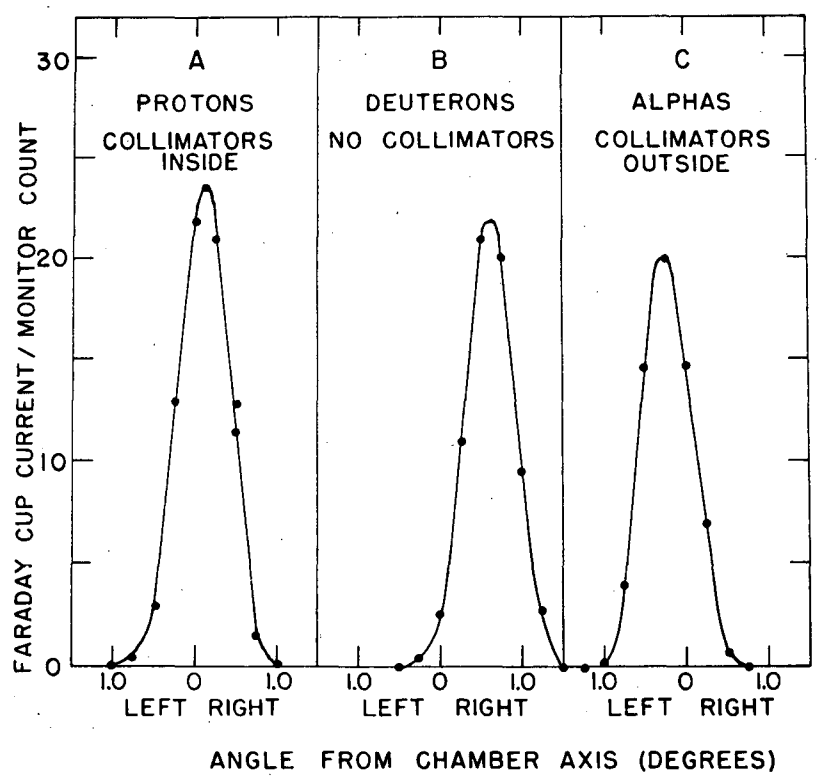

Fig. 5. Beam profiles. Notice that the half width of each curve is 0.75°, independent of the type of particle and of the position of installation of the carbon collimators.

The second and third discriminators were set as low as practicable just above the noise level. The absorber was adjusted to maximize the CCA's, or, in the language of the trade, "the counter was set on the peak." A discriminator curve for Chamber 1 was obtained by determining the number of CCA's as a function of the first discriminator. A typical curve is shown in Fig. 6a. Under normal conditions it was usual to pick the operating point near the upper end of the plateau, for example, N on that graph. Figure 6b illustrates proton and deuteron discriminator curves taken with the same high voltage and amplifier gain. In order to discriminate against protons while counting deuterons, one should choose an operating point like D.

After the first discriminator was set at the desired bias level, the second was varied and the number of CCA's determined to obtain a Chamber 2 discriminator curve. A typical plot, depicted in Fig. 6c, does not show a plateau. The slope of the first portion of this curve may be understood when one considers that variation of the bias level unavoidably changes the ΔR in which the particles may stop and still be identified as a CCA. To insure fairly good resolution (i.e., a reasonably small range-window width) without the necessity of operating in a region where slight drifts in amplifier gain, counter high voltage, etc., would cause serious variation in counting efficiency, it was usual to choose an operating point near the end of the less steep portion of this curve.

Since the third counter was to act simply as a yes-no device, its discriminator was set as low as possible--not so low, however, that electron pulses were counted.

When the range of the particle group to be detected was considerably greater than that for any other group emitted from the target, it represented a saving in time to count integrally. In this mode of operation the CC's include, roughly speaking, all particles with a range greater than R_1, and the CCC's all particles with a range greater than R_2, where $R_2 > R_1$. This statement is, in fact, incorrect. Since the rate of energy loss is a decreasing function of residual range (at nonrelativistic energies) it was impossible with practical bias settings to avoid

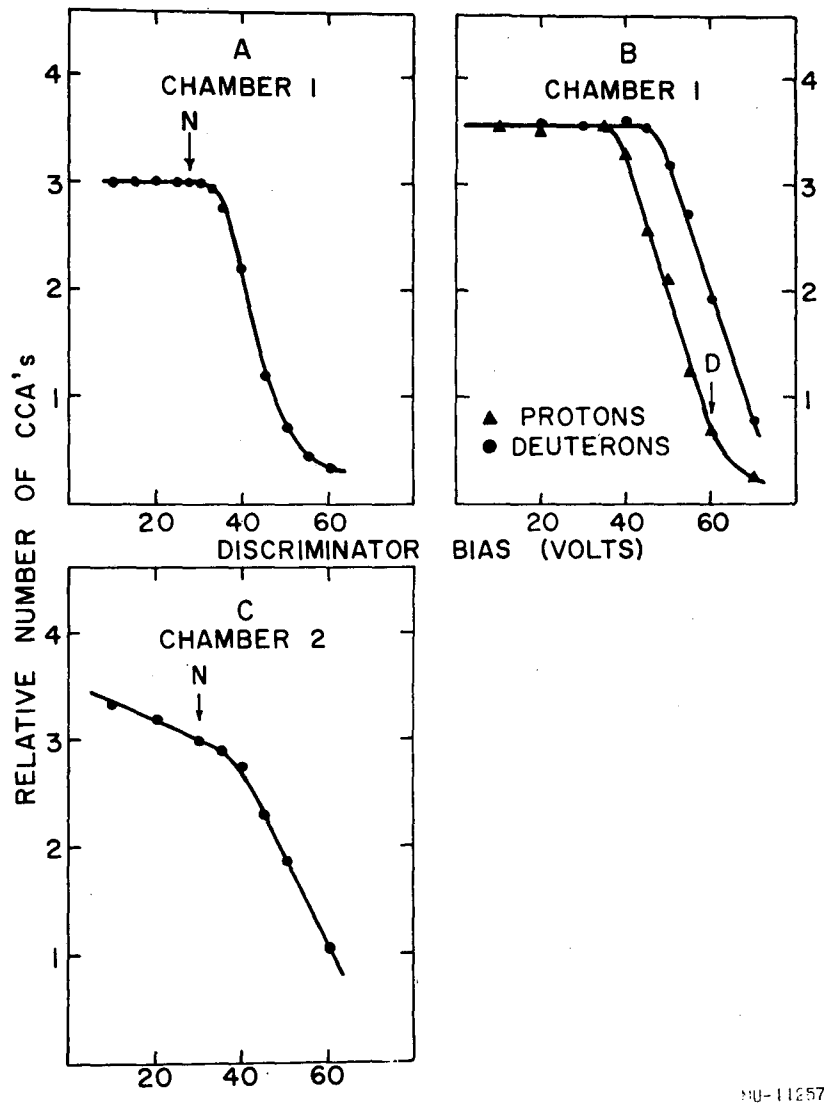

Fig. 6. Differential discriminator curves. The data for A and C were taken with alpha particles. The difference in pulse height between protons and deuterons is indicated in B.

a high-range cutoff. The excuse for using the name "integral counting" is that the range acceptance width could be made as large as 50 mg/cm^2. The differential window width on the other hand, was approximately 3 mg/cm^2. The procedure followed to find the optimum bias settings in this case is described below.

With all three discriminators set low, the counter was set suitably below the peak so that the elastic particles were passing into and through the third chamber. Through variation of the bias setting, first for Chamber 1 and then for Chamber 2, the number of CC's (CCC's showed the same general behavior) was obtained as a function of bias voltage. Typical integral bias curves are shown in Figs. 7a and 7b. Normal operating points would be as marked, namely, on the flat portions of the curves as near the noise level as possible. The third discriminator also was set as low as practicable. With the bias settings chosen, correct integration action was checked by plotting the number of CC's as a function of absorber in the region of the elastic peak. See the upper curve of Fig. 8.

For integral counting, provided losses due to the high-range cutoff are avoided, detection efficiency is 100%. That is, the total number of particles N_t in an elastic peak is just the number of CC's recorded at any suitable absorber setting below the peak. The differential data, however, are not so directly related to N_t. At any absorber R the number of CCA's N(R) is the number of particles with range between $R-\Delta R/2$ and $R + \Delta R/2$, where ΔR is the window width or "range bite" of the counter. After the determination of N(R) throughout the region of the peak, one can write

$$\int_{\text{peak}} N(R)\, dR = \Delta R \int dN = N_t\, \Delta R.$$

Thus

$$\Delta R = \frac{\text{Area under the peak (taken differentially)}}{\text{Total number of particles in peak (taken integrally)}}.$$

Once the range bite has been determined, N_t for any other differential peak can be obtained by dividing its area by this number. The value of ΔR was generally about 3.1 mg/cm^2, but of course it varied from run

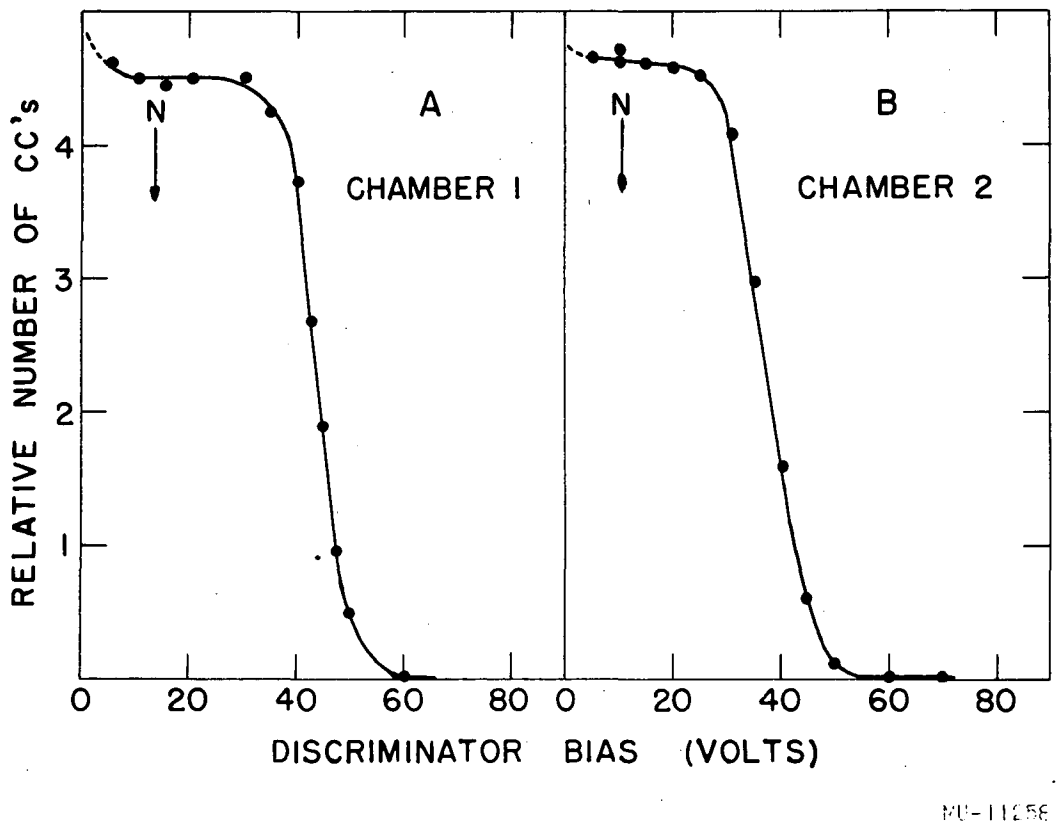

Fig. 7. Integral bias curves. The data were taken with protons.

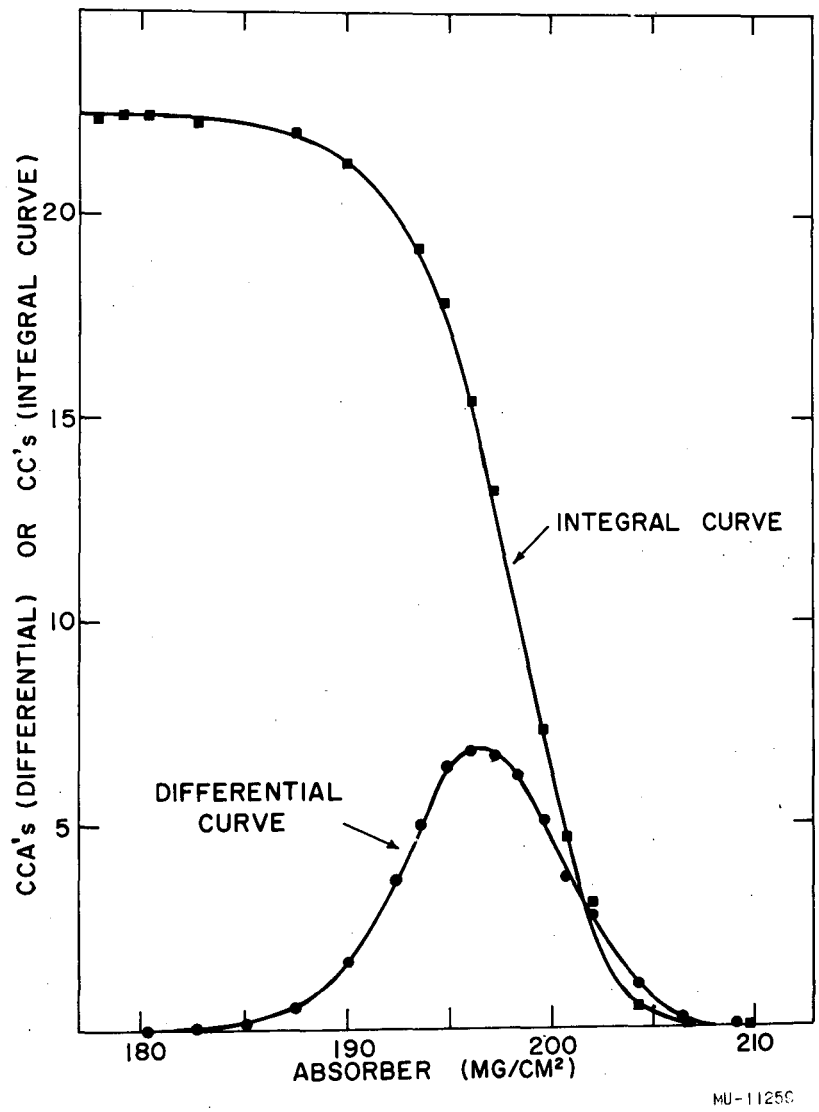

Fig. 8. Typical differential and integral curves for obtaining the range bite of the counter. The data were taken with protons.

to run owing to differences in bias settings, etc. A typical determination of the range bite is illustrated in Fig. 8, which also shows the relationship between differential and integral counting.

H. The Measurement of Differential Cross Sections

For each cross section measured, the counter and target were set at the desired angles and the beam level adjusted to give suitable counting rates, that is, singles rates in each chamber not in excess of 400 or 500 per second.

Scanning of the charged-particle spectra was done, and data for most of the cross sections reported were obtained differentially. In the absorber region of interest the number of CCA's for a suitable fixed amount of incident beam was determined as a function of absorber. It was usual to measure points every 2.4 mg/cm^2 across a peak and then, to better determine the shape, the middle points in each interval were taken. As a result, therefore, data every 1.2 mg/cm^2 were obtained. This alternating procedure was adopted as protection against gradual shifts in the beam energy. Slight though these might be, if they went unobserved the peaks would be erroneously widened or narrowed, introducing errors in the peak areas.

After checks had been made at several angles to assure that the elastic proton group was well separated from inelastic events, the data for this cross section were taken integrally. In order to avoid prolonged deuteron bombardments and the consequent high radiation level in the laboratory, a large part of the elastic deuteron data was taken in the same way. Here, too, differential scanning was carried out at a sufficient number of angles to verify the accuracy of the integral data. To verify that the number of CC's so obtained included all of the desired peak and a negligible number of other particles, a series of about four points were taken, with absorber values differing by steps of 2.4 mg/cm^2, in the region below the peak being integrated. The constancy of the number of CC's obtained and the near equality of the CC's and CCC's implied that the low side of the peak was, indeed, "clean" and that,

furthermore, no loss of counts was occurring because of the high-range cutoff. One additional point, taken at an absorber value just greater than that of the upper edge of the peak, indicated that the peak was "clean" on the high side.

To avoid systematic errors due to drifts in the electronic equipment--during a day, over a run, or from run to run--frequent checks of the cross-section determinations were made. At least one point taken during the preceding day (or run) was repeated the following day (or run). Furthermore, the various angles were measured in random or at least alternate sequence.

Target-out backgrounds (except for the deuteron bombardments) were negligible except at angles less than 15° or greater than 130°. These were determined where necessary either immediately after the target-in data for that angle or (more often) after the completion of all the target-in data for a given run. The latter procedure was adopted to avoid possible errors in the relative cross-section shapes due to inhomogeneity and inexact replacement of the target. This eventuality was thought to be more likely than time variation of the background.

I. Reduction of Data

The expression for the differential cross section in the laboratory frame may be written in the form

$$\left(\frac{d\sigma}{d\Omega_L}\right)_{\theta_L} = \frac{X'}{n\,N\,\Delta\,\Omega},$$

where X' is the number of particles emitted from the target into the solid angle $\Delta\Omega$ per microcoulomb of incident beam,

$n = 1/ze$ is the number of beam particles per microcoulomb,

z, the charge of the bombarding particle, is 1 for protons and deuterons and 2 for alpha particles,

e is the electronic charge in microcoulombs,

N is the number of target nuclei per square centimeter of the target,

and $\Delta\Omega$ is the solid angle within which the scattered particles are detected by the counter.

The nuclear target density can be expressed in terms of constants and the quantities actually measured,

$$N = \frac{LT}{M \cos \theta_T} ,$$

where L is Avogadro's number,

T is the thickness of the target in grams/cm^2 (in case the target is not completely composed of the target nucleus, this quantity is to be taken as the areal density of that nucleus only),

M is the atomic weight of the target nucleus atom,

and θ_T is the angle between the normal to the target and the direction of the incident beam.

After transformation to the center-of-mass frame the expression becomes

$$\left(\frac{d\sigma}{d\Omega}\right)_\theta = \left[Gz\right] \cdot \left[\frac{Me}{L}\right] \cdot \left[\frac{\cos \theta_T}{T\ \Delta\Omega} \quad X'\right] ,$$

where $G = d\Omega_L/d\Omega$, and the center-of-mass angle θ corresponds to the laboratory angle θ_L. Letting $X' = X/Q$

and $X = A/B$ for differential counting, or

$X = C$ for integral counting,

where B is the range bite of the counter,

A is the area under the peak for a charge of Q microcoulombs collected at each absorber setting, and

C is the number of CC's counted for a charge of Q microcoulombs, we have the equation in the form most convenient for computation,

$$\left(\frac{d\sigma}{d\Omega}\right)_\theta = \left[Gz\right] \cdot \left[\frac{Me}{L}\right] \cdot \left[\frac{\cos \theta_T}{T\ Q\ \Delta\Omega} \cdot X\right] .$$

The errors involved in a cross-section measurement are readily obtained in the usual way. The quantities in the first bracket are

errorless, while those in the second are fundamental physical constants whose errors are negligible in comparison with the other errors involved in the experiments. Thus we have

$$\frac{\delta\left(\frac{d\sigma}{d\Omega}\right)}{\frac{d\sigma}{d\Omega}} = \left\{\left[\frac{\delta(\cos\theta_T)}{\cos\theta_T}\right]^2 + \left[\frac{\delta T}{T}\right]^2 + \left[\frac{\delta Q}{Q}\right]^2 + \left[\frac{\delta(\Delta\Omega)}{\Delta\Omega}\right]^2 + \left[\frac{\delta X}{X}\right]^2\right\}^{1/2}.$$

These errors are of two types, those which affect the shape of the cross sections and those which affect only the absolute values, that is, those which are common to all measurements regardless of angle. For each of the quantities θ_T, T, Q, $\Delta\Omega$ and X, therefore, the errors involved are discussed from these two points of view.

The target angle took only two nominal values, 0° and 45°. The reproducibility of the 0° setting was checked before each run and found to be $\pm 0.1^\circ$. Unfortunately it was not easy to check the 45° position with sufficient precision. A conservative estimate of the error was taken as $\pm 0.25^\circ$. Thus $\frac{\delta(\cos\theta_T)}{\cos\theta_T}$ is 3×10^{-6} at 0° and 4.1×10^{-3} at 45°. The error in absolute value due to the error in the target angle is therefore $\pm 0.41\%$. The error in relative cross section due to target angle is virtually zero, however, since the target angle was not adjusted for whole series of points--in fact all the elastic proton data were taken with one target angle setting.

The target thickness was determined to be $4.69 \pm .02$ mg/cm^2. The absolute error due to the target is therefore $\pm 0.37\%$. In addition, a relative error of 1% has been conservatively allowed for possible target inhomogeneity. By actual test,* it is probable that the target was more nearly homogeneous than has been allowed.

The charge (amount of incident beam) collected at a point was calculated from the relation $Q = VCd$, V being the voltage at full scale on

---

* The number of integral counts for the elastic proton group at 40° was measured with the target moved slightly between each determination. All the numbers were within the 1% counting statistics.

the recorder, C the capacity of the condenser used, and d the number of "dumps" of the electrometer. The recorder calibration was checked before and after each run by comparing its deflection for voltages also measured with a Leeds and Northrup potentiometer. These calibrations were estimated to be accurate to 0.1% and were in fact constant to within 0.3% over a period of several months. The condensers used were compared with a secondary standard condenser of 1.043 ± 0.005 microfarads by the method of charge-sharing. Their values were found to be constant within 0.3% over a period of several months. The number of dumps, being confined to integral values, was exact. In summary, for the relative cross sections $\frac{\delta Q}{Q} = \pm 0.54\%$ and for absolute calibration there is an additional 0.5% error.

The detector collimator was a round hole of radius 0.1252 ± .0005 in. at a distance of 12.284 ± .025 in. from the target. These dimensions were determined by traveling microscope and 1/64-in. rule, respectively. The solid angle $\Delta\Omega$ was therefore $(3.265 \pm 0.039) \times 10^{-4}$ steradian and its fractional error 0.90%. As effects due to the finite size of the beam spot are small, the solid-angle error is one of absolute magnitude only.

By far the greatest source of error was in the determination of X, the number of particles in a peak. The origin of this uncertainty depends on the method of counting. To consider integral counting first, contributions to the error in X come from statistics, background under the peak, counts above the peak, and counts below the peak. A generalized integral determination yields the numbers N_L and n_L counting below the peak and N_H and n_H above the peak, where the N's refer to the CC's and the n's to the CCA's. If the ideal case $N_H = n_H = n_L = 0$ does not prevail there are three extreme explanations of the data.

(a) There is a second peak at slightly greater range than the one under consideration. Since it contributes to both N_L and N_H, the correct value of X is $N_L - N_H$.

(b) There is a second peak at considerably greater range than the one under consideration. If it contributes to N_H but not N_L, the correct value of X is N_L.

(c) A general background level (for example, initiated by neturons or due to multiple scattering) is interfering. In such a case if one assumes it to be constant with respect to absorber the correct value of X is $N_L - N_H$. To first order, allowance for a possible linear variation can be made by taking $X = N_L - \frac{n_L}{n_H} N_H$.

Since there is no way, within the framework of integral counting, to correct for an overlapping peak on the low side, the absence of such an effect must be verified differentially before integration is considered. Because of the uncertainty in the exact correction to be applied, the number of CC's was taken to be N_L. The probable error assigned was $^{+0}_{-(1/2)} N_H$. The statistical error is $\pm 0.67\sqrt{\Sigma N_L}$. These were combined quadratically to give $\frac{\delta X}{X}$.

The determination of X from differential data can be a much more involved process. After the plotting of a differential spectrum a smooth curve was drawn visually through the points, whose statistical errors were kept in mind. Ordinates were read every 1 mg/cm^2 across the region of interest of the spectrum and the area under the curve was evaluated by use of the trapezoidal rule.* Where peaks overlapped or an obvious background was present the total ordinate was distributed among the individual features so that each would have a smooth and logical shape.† The results of such a partition are shown in Fig. 9 for protons on beryllium at $\theta_L = 21^\circ$. Finally, this area was divided by the counter range bite to yield X.

---

* It was found that the trapezoidal rule and the more accurate Simpson's 1/3 rule gave the same result within the statistical errors of the data. Since trapezoidal-rule computations are the more readily accomplished, this method was used.

† From the theory of range straggling[35] the shape of a peak should be approximately Gaussian, with a broader tail on the low range side. Cleanly resolved peaks agreed with expectations.

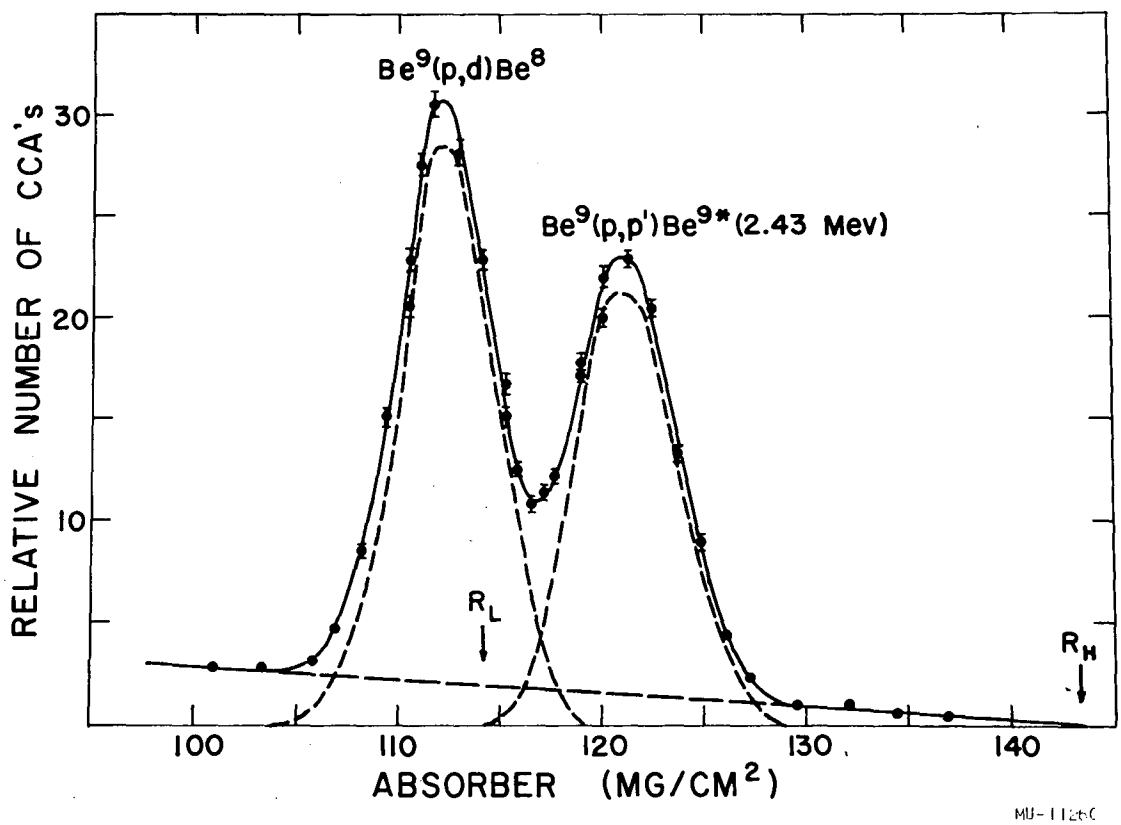

Fig. 9. The separation of overlapping peaks and backgrounds. (The significance of the arrows is explained in the Appendix.)

Under these conditions the error in X includes contributions from counting statistics, background under the peak, overlapping of peaks, variation in peak width, and determination of range bite. A short discussion of each follows.

Since the area integral was replaced by the finite summation

$$A = \int_{peak} N(R)\, dR = \sum_{i=0}^{m} N(R_i)\, \Delta R_i,$$

the statistical error in the integral may be written

$$\left(\frac{\delta A}{A}\right)_{stat} = 0.67\left\{\sum_{i=0}^{m} \left[\sigma_N(R_i)\right]^2 \Delta R_i^{\,2}\right\}^{1/2} = 0.67\left\{\sum_{i=0}^{m} N(R_i)\Delta R_i^{\,2}\right\}^{1/2}.$$

This expression was evaluated for several peaks and the relative error in the area found to have the upper limit.

$$\left(\frac{\delta A}{A}\right)_{stat} \leq \frac{0.060}{\sqrt{p/64}},$$

where p is the number of counts at the peak. To reduce the amount of computation necessary the statistical error in all peaks was conservatively estimated by assuming equality.

Background under elastic peaks was virtually nonexistent. Background under the 2.43-Mev inelastic peaks and the $Be^9(p, d)Be^8$ peak was undoubtedly due to the reactions $Be^9(x, nx')Be^8$. By means of the analysis outlined in the Appendix the angular dependence of these backgrounds was found. The distributions were smooth functions of angle within 10%. With this internal-consistency estimate of background errors, the error in a peak due to background effects was considered to be ±10% of the background subtracted. The error due to background subtraction for peaks corresponding to more highly excited states would be considerably greater.

At those angles where peaks overlapped one another, additional error was introduced. Extreme estimates of the areas of the unresolved peaks were then made and their deviations from the most reasonable areas treated as probable errors. The uncertainty from this effect was

thus most conservatively treated. The very large errors in the inelastic cross sections at forward angles resulted from the overlap of elastic events.

The net area of each peak was divided by its net peak height to determine the half width of an equivalent triangular peak. From kinematical considerations and the theory of range straggling, such half widths would be expected to show a smooth variation with scattering angle except where the target angle was changed from 0° to 45° or from transmission to reflection. From their fluctuation about smooth curves an error of ±3% due to peak-width variation was deduced. As already mentioned, small energy shifts during data taking could distort the peak widths observed. Although precautions were taken to avoid this occurrence's passing unnoticed, an error of this magnitude could have been present. Including it gives a conservative estimate of the accuracy of the measurements.

Finally, the determination of X by the differential method requires the measurement of the range bite B. Since the bite is evaluated as the ratio of an integral count and a differential peak area, the error in its magnitude was computed from the preceding considerations. By use of the elastic scattering from gold for this determination, errors in it due to background and overlap were minimized. During a run the range bite remained the same (as evidenced by the consistency of the check points taken each day). Thus, this error is one of absolute value only.

To further illustrate the method of calculation of the differential cross sections and to exemplify the magnitude of the errors involved, two sample computations follow--one derived from differential data and one measured by integration.

For the observation of the 2.43-Mev inelastic alpha particles at a laboratory angle of 69.8° the target angle was 42.8°. The amount of incident beam for each point taken was 3.31 microcoulombs. The area under the differential curve was 238 x 64 counts x mg/cm^2, while over the same region the best estimate of the background due to the $(\alpha, n\alpha')$ reaction was 45 x 64 counts x mg/cm^2. The number of counts at the

peak of the inelastic distribution was 40.4 x 64. Target-out background was negligible at this angle of scattering. The range bite of the counter during this run was 3.23 ± .10 mg/cm^2. The error due to overlap of the elastic peak was estimated to be ± 1.2 x 64 counts x mg/cm^2.

From the above data:

$$X = \frac{(238 - 45) \times 64}{3.23} = 3820 \text{ counts},$$

$$\left(\frac{\delta X}{X}\right)_{stat} = \frac{0.060}{\sqrt{40.4}} = 0.94\%,$$

$$\left(\frac{\delta X}{X}\right)_{bkgd} = \frac{(0.10)\,(45)}{(238 - 45)} = 2.33\%.$$

From the kinematics of the reaction, for $\theta_L = 69.8^\circ$, $\theta = 95.5^\circ$ and G = 0.800. Thus we have

$$\left(\frac{d\sigma}{d\Omega}\right) = \left[(.800)\,(2)\right]\left[\frac{(9.013)\,(1.602 \times 10^{-13})}{6.023 \times 10^{23}}\right] \times$$

$$\left[\frac{\cos 42.8^\circ}{(4.69 \times 10^{-3})\,(3.31)\,(3.265 \times 10^{-4})}\right] \times 3820,$$

$$\frac{\delta\left(\frac{d\sigma}{d\Omega}\right)}{\frac{d\sigma}{d\Omega}} = \left[(.010)^2 + (.0054)^2 + (.0094)^2 + \right.$$

$$\left. (.0233)^2 + \left(\frac{1.2}{193}\right)^2 + (.030)^2\right]^{1/2} = .041,$$

so that $\left(\frac{d\sigma}{d\Omega}\right)$ = 2.13 ± .09 millibarns/steradian, where the absolute value is subject to an additional 3.3% error.

For the observation of the elastic scattering of protons at $\theta_L = 60.1^\circ$ the target angle was 42.5°. The mean number of doubles below the peak was 200 x 64, while the number above the peak was 8.4 x 64. The amount of beam incident for these determinations was 1.102 microcoulombs.

From the kinematics, $\theta_L = 60.1^\circ$ corresponds to $\theta = 65.7^\circ$--G = 0.900. Then

$$X = 200\ (64) = 1.28 \times 10^4,$$

$$\left(\frac{\delta X}{X}\right)_{stat} = \pm .0051,$$

$$\left(\frac{\delta X}{X}\right)_{bkgd} = \begin{matrix} +\ 0 \\ -\ .021 \end{matrix}.$$

Subject to an additional absolute error of 1.2%, we have

$$\frac{d\sigma}{d\Omega} = 12.0 \begin{matrix} +\ .14 \\ -\ .28 \end{matrix} \text{ mb/sterad.}$$

From these representative data one should not conclude that the integral method is more accurate than the differential method. One should rather conclude that the elastic data are more accurate than the inelastic because of the absence of an underlying continuum in the first case.

To these quantitative errors must be appended several errors whose exact magnitudes cannot be estimated. The first of these is due to target impurities. As already stated, somewhat less than 1% oxygen contamination was present in the target. At forward angles the elastic scattering from this oxygen was included unavoidably in the beryllium elastic groups. At the more backward angles inelastic scattering from oxygen may have interfered with the determination of the inelastic scattering of alpha particles from beryllium. For want of a quantitative estimate of the errors so introduced, uncertainties from this effect have been neglected.

Two other sources of error are manifestations of changes in the cyclotron operating parameters. Variation of oscillator power can change the beam energy--at low power the energy is somewhat lower than at high power. In order to maintain reasonable counting rates at the various angles of measurement the beam was adjusted to low intensity at small angles and higher-than-average intensity at large angles. These order-of-magnitude changes were, by necessity, made by

adjustment of oscillator power. As a consequence, throughout these investigations, the smaller angles were measured at a beam energy systematically lower than average while large-angle data were taken at higher energies. The total variation of energy in this way may have been as much as 0.5 Mev for the 48-Mev alpha particles, with similar percentage changes for the other projectiles. Since no information that would permit compensation for such an effect is available, no adjustments have been made.

The second uncertainty, also due to variation of the cyclotron operating conditions, is that caused by changes in the direction of travel of the incident beam. It was observed during alignment that the beam position at the target could be shifted by as much as 1/8 in. (equivalent to a shift in beam direction of as much as 0.6°) by gross changes in the deflector voltage and ion source position. During data taking, however, the operating crew never allowed conditions to drift so widely from those under which chamber alignment and beam position measurement had been carried out. Such variations would have been most serious in the measurement of the alpha-particle cross sections. The self-consistency of the structure in these graphs is good evidence that any such effects were small.

IV. RESULTS

A. Proton Bombardments

The complete charged-particle spectrum was measured at 25° and 65° in the laboratory frame. The 65° results are shown in Fig. 10. Oxygen contamination of the target gives rise to the elastic oxygen peak labeled I. Peak II consists of protons elastically scattered from Be^9. Peak V is a deuteron group from the reaction $Be^9(p, d)Be^8$, where the residual nucleus is left in its ground state. Peak VI, at least in part, consists of deuterons from the same reaction where Be^8 is left in its broad excited state at 2.9 Mev. Peak IV, part of VI, and the rise at 15 mg/cm^2 are proton groups corresponding to the levels in Be^9 at 2.43, 4.8, and 6.8 Mev. Owing to the presence of the ground-state deuteron group V the level at 3.1 Mev could not be verified. The very small peak labeled III can be interpreted as corresponding to a level in Be^9 at 1.8 Mev. The maximum range of protons from the three-body reaction $Be^9(p, np')Be^8$ is shown by the arrow to the right of peak IV. All ranges less than this are kinematically possible.

Data taken at 25° showed no major differences. The elastic peak was, of course, very much larger, thereby preventing the observation of the 1.8-Mev peak. The 4.8-Mev level did not appear to be so prominent; however, this may have been due to masking by a considerable increase in the general continuum. The 6.8-Mev level clearly manifested itself at this angle where the inelastic proton energy was great enough to permit scanning below the peak.

The group corresponding to elastic scattering was measured by the integration method at 5° and 10° intervals from 7° to 167° in the laboratory frame. In addition, the peak was examined differentially at several angles throughout this range. In each case good agreement was obtained with the integral data. Where visible, the oxygen elastic peak was generally about 1% of the beryllium peak. The cross sections for elastic scattering obtained from this data are shown by the solid points of Fig. 11. The Rutherford cross section is shown by the solid curve,

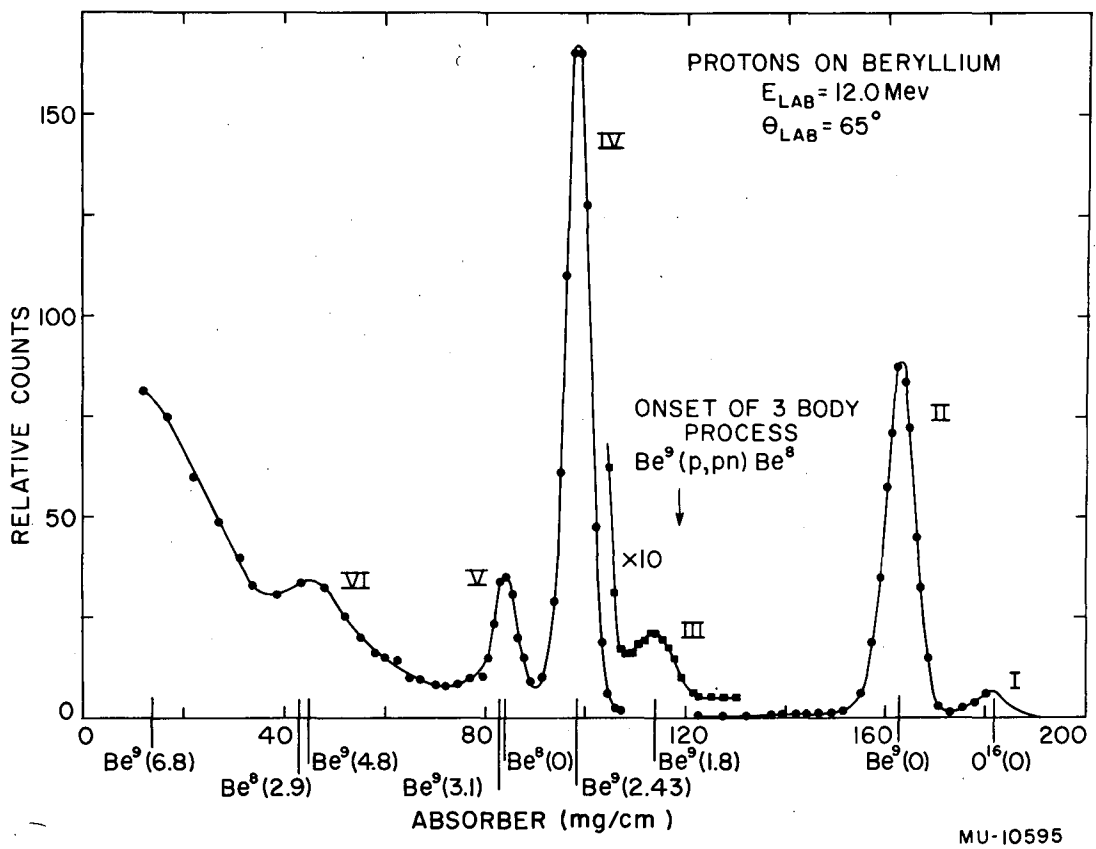

Fig. 10. Charged particles from the proton bombardment of beryllium. The short leaders along the abscissa indicate the expected positions of the peaks corresponding to the final states by which they are labeled. The numbers in parentheses are excitation energies.

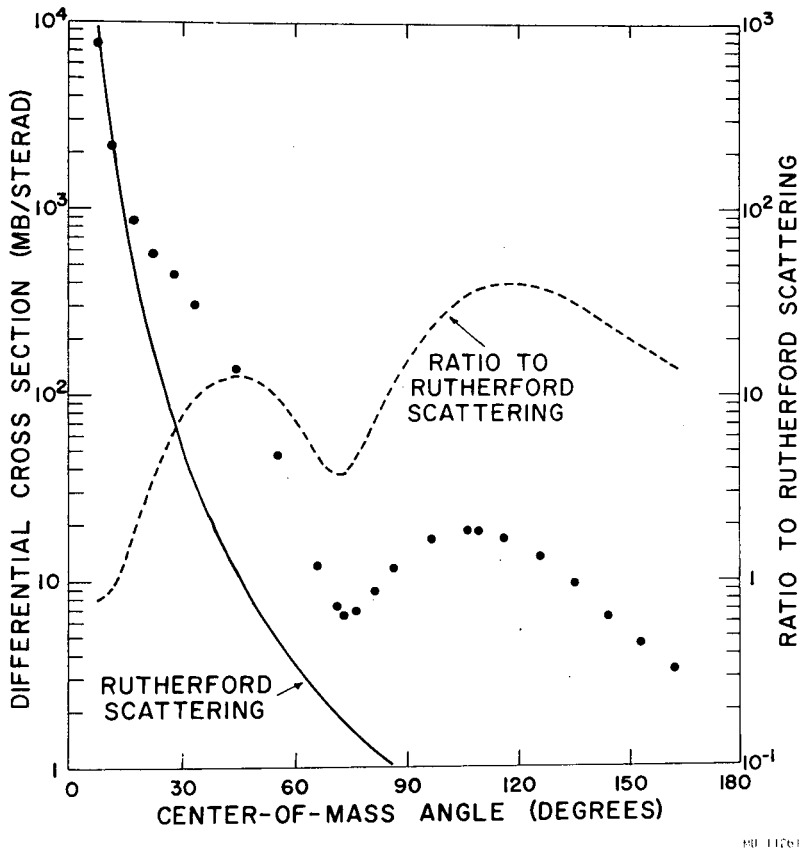

Fig. 11. The differential cross section for elastic proton scattering by beryllium at a laboratory energy of 12 Mev. Experimental errors are less than the size of the points.

while the ratio to Rutherford scattering is indicated by the dashed curve. The data are also listed in Table I.

The very small peak labeled III in Fig. 10 has been examined in detail at four angles from 40° to 90° in the laboratory system. As mentioned, its presence at 25° could not be clearly established, owing to the overwhelming magnitude of the elastic cross section. Poorer resolution due to the use of a reflection target at angles beyond 90° precluded the possibility of detecting such a small peak. Nevertheless, from the variation of its position with angle over the range mentioned, it is clear that it is a proton group from an initial nucleus of mass 9. If the peak is treated as evidence of a level in Be^9, the latter would have an excitation energy of 1.83 ± .05 Mev, and a half width of ~0.2 Mev. The differential cross section for its formation by inelastic proton scattering (12 Mev) would be 0.15 ± .06 mb/sterad at $\theta = 71.5^{\circ}$, 0.16 ± .08 mb/sterad at 97.0°, and 0.09 ± .03 mb/sterad at 55.4°. For comparison, at the same angles, the cross section for the formation of the 2.43-Mev level is about 9 mb/sterad.

The region of the differential spectrum in the vicinity of the 2.43-Mev inelastic protons and of the pickup deuterons was measured at some twenty angles from 7° to 167° in the laboratory frame. That the latter were deuterons was strongly suggested by the range-angle dependence of the position of the group. This identification was conclusively confirmed by the shape of the Chamber 1 discriminator curve for this peak. The differential cross sections for the inelastic scattering and for the pickup reaction are given in Tables II and III and shown in Fig. 12 and 13. Experimental points are shown with their probable errors. The significance of the curves is discussed in a later section. The total integrated cross section for the reaction $Be^9(p, d)Be^8$ is 40 millibarns. For the inelastic scattering $Be^9(p, p')Be^{9*}$ (2.43 Mev), the same quantity is 111 millibarns.

Considerable three-body breakup was observed in the proton bombardments. While such a reaction does not manifest itself by the presence of a discrete-energy particle group, it can nevertheless be studied through the methods outlined in the Appendix. The results of

Table I

Differential cross sections and their ratios to Rutherford cross sections for the elastic scattering of 12-Mev protons by beryllium

θ (degrees)	$d\sigma/d\Omega$ (mb/sterad)	$\left(\frac{d\sigma}{d\Omega}\right)\Big/\left(\frac{d\sigma}{d\Omega}\right)_c$
7.9	7840 ± 100	0.801 ± .010
11.2	2160 ± 30	0.890 ± .012
16.8	876 ± 11	1.811 ± .023
22.3	580 ± 7	3.69 ± .045
27.7	453 ± 15	6.75 ± .22
33.3	310 ± 3	9.46 ± .09
44.2	139 ± 2	12.63 ± .16
55.0	$47.3^{+.6}_{-.2}$	$9.74^{+.12}_{-.04}$
65.7	12.0 ± .2	4.71 ± .08
70.9	$7.18^{+.09}_{-.25}$	$3.69^{+.05}_{-.13}$
73.0	$6.53^{+.08}_{-.31}$	$3.72^{+.05}_{-.18}$
76.1	$6.87^{+.07}_{-.25}$	$4.51^{+.05}_{-.16}$
81.3	$8.75^{+.11}_{-.41}$	$7.15^{+.09}_{-.33}$
86.4	$11.71^{+.15}_{-.54}$	$11.65^{+.15}_{-.54}$
96.5	$16.48^{+.15}_{-.27}$	$23.2^{+.2}_{-.4}$
106.2	$18.7^{+.2}_{-.5}$	$34.7^{+.4}_{-.9}$
109.0	18.7 ± .6	37.3 ± 1.2
115.9	$16.8^{+.2}_{-.4}$	$39.0^{+0.5}_{-1.0}$
125.5	$13.4^{+.15}_{-.3}$	$38.0^{+.5}_{-.9}$

Table I (cont'd)

θ (degrees)	$d\sigma/d\Omega$ (mb/sterad)	$\left(\frac{d\sigma}{d\Omega}\right)/\left(\frac{d\sigma}{d\Omega}\right)_c$
134.8	$9.58 \begin{smallmatrix} +.11 \\ -.15 \end{smallmatrix}$	$31.7 \begin{smallmatrix} +.4 \\ -.5 \end{smallmatrix}$
144.0	$6.43 \begin{smallmatrix} +.08 \\ -.18 \end{smallmatrix}$	$23.9 \begin{smallmatrix} +.3 \\ -.7 \end{smallmatrix}$
153.1	$4.62 \begin{smallmatrix} +.06 \\ -.19 \end{smallmatrix}$	$18.8 \begin{smallmatrix} +.2 \\ -.8 \end{smallmatrix}$
162.1	$3.31 \pm .23$	14.3 ± 1.0

Table II

Differential cross sections for the inelastic scattering (2.43-Mev level) of 12-Mev protons by beryllium.

θ (degrees)	$d\sigma/d\Omega$ (mb/sterad)
8.0	$13.5^{+2.8}_{-.5}$
11.3	$15.1^{+3.1}_{-1.5}$
13.6	$15.0^{+.7}_{-.6}$
20.2	$16.5^{+.7}_{-1.1}$
23.7	14.9 ± .6
28.4	15.7 ± .35
36.1	15.0 ± .4
45.3	14.1 ± .35
53.4	12.9 ± .45
63.1	11.6 ± .4
68.5	10.5 ± .2
80.0	8.70 ± .27
87.3	7.69 ± .24
94.9	7.11 ± .24
103.2	$6.84^{+.24}_{-.21}$
109.9	6.44 ± .21
116.9	6.28 ± .21
126.2	$5.82^{+.21}_{-.18}$
135.5	5.09 ± .18
144.7	4.50 ± .18
153.6	4.20 ± .15
164.2	4.05 ± .24

Table III

Differential cross sections for the reaction $Be^9(p, d)Be^8$ at 12 Mev.

θ (degrees)	$d\sigma/d\Omega$ (mb/sterad)
8.3	$20.5^{+2.5}_{-.8}$
11.6	$20.7^{+4.1}_{-2.0}$
14.1	$21.6^{+.9}_{-.7}$
20.9	$19.2 \pm .8$
24.5	$15.2 \pm .6$
29.3	$11.8 \pm .3$
37.2	$7.50 \pm .21$
46.7	$4.23^{+.13}_{-.11}$
55.0	$3.03^{+.16}_{-.11}$
64.9	$2.06^{+.12}_{-.07}$
70.4	$1.57 \pm .05$
82.0	$1.28^{+.09}_{-.05}$
89.4	$1.42^{+.08}_{-.05}$
97.0	$1.58^{+.07}_{-.14}$
105.3	$1.36^{+.17}_{-.06}$
112.0	$1.34 \pm .13$
118.8	$1.60^{+.12}_{-.15}$
128.0	$1.25^{+.11}_{-.05}$
137.1	$1.11^{+.13}_{-.06}$
146.0	$0.92 \pm .13$
154.7	$0.91 \pm .14$
164.8	$1.52 \pm .55$

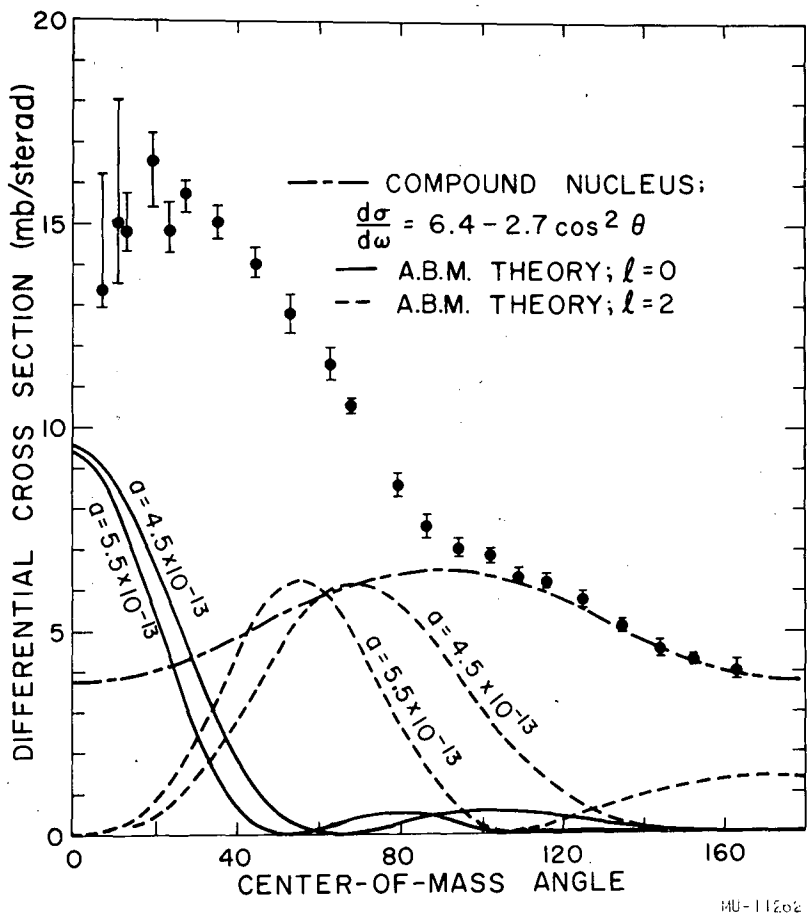

Fig. 12. The differential cross section for the formation of the 2.43-Mev state of beryllium by inelastic proton scattering. The laboratory energy was 12 Mev.

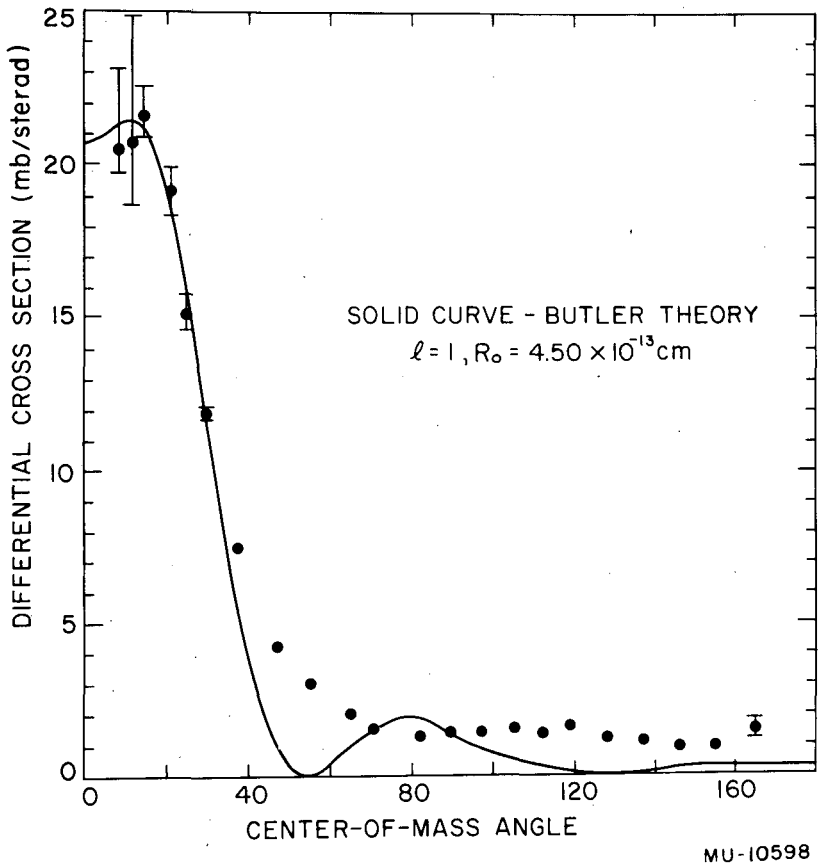

Fig. 13. The differential cross section for the reaction $Be^9(p,d)Be^8$ at 12 Mev.

such an analysis for the reaction $Be^9(p, np')Be^8$ are shown in Fig. 14. The left-hand ordinate gives the differential cross section for the formation of the Be^8 ground state and the scattering of the proton through an angle θ where the available kinetic energy has been shared in such a way that, in the center-of-mass system, $0.90E_{p'}^{max} \leq E_{p'} \leq E_{p'}^{max}$. If the assumption is made that the energy is shared statistically, the differential cross section for the scattering of the proton through angle θ with any energy is given by the right-hand ordinate. Under such an assumption the total cross section for the "neutronization" of Be^9 by 12-Mev protons is 185 millibarns.

B. Alpha-Particle Bombardments

The results for 48-Mev alpha particles incident on beryllium are given in the following paragraphs. Complete alpha-particle spectra were taken at laboratory angles of 14.5°, 29.8°, and 62.5°. The results for $\theta_L = 62.5°$ are shown in Fig. 15. Data at the other angles were essentially the same. Peak I contains alpha particles scattered elastically from beryllium. The second peak corresponds to the 2.43-Mev level, while Peaks III and IV correspond to the more highly excited states at 6.8 and 11.3 Mev respectively. A small peak arising from elastic scattering from oxygen was present but occurs at 123 mg/cm^2 of absorber and is therefore not shown on the graph. It is apparent that identification of weak particle groups corresponding to levels at 1.8 and 3.1 Mev was precluded owing to insufficent resolution in the presence of the near-by intense 2.43-Mev peak. There seems to be no clear evidence of the 4.8- and 7.9-Mev levels, although conditions for their observation were more favorable. If these levels are broad or only weakly excited their presence may have been masked by the prevailing continuum. No attempt was made to observe protons in these measurements. An (α, p) reaction leading to the ground state of B^{12} would yield 30-Mev protons. The absorber changer was not loaded with sufficiently thick absorbers to permit the detection of such particles if they existed.

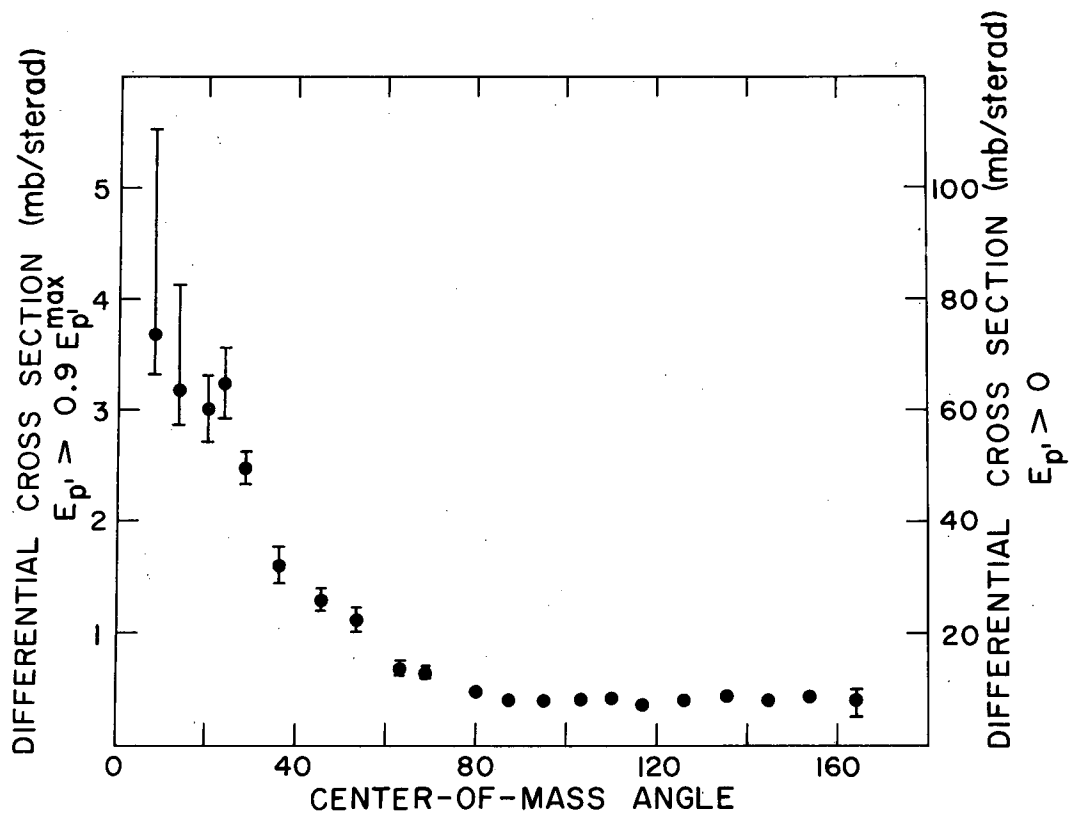

MU-11263

Fig. 14. The differential cross section for the reaction $Be^9(p, np')Be^8$ at a laboratory energy of 12 Mev. The values on the left for $E_{p'} > 0.9\ E_{p'}^{max}$ were measured directly. Those on the right follow if the available energy is shared statistically among the products. Notice that the abscissa is the angle of scattering of the proton.

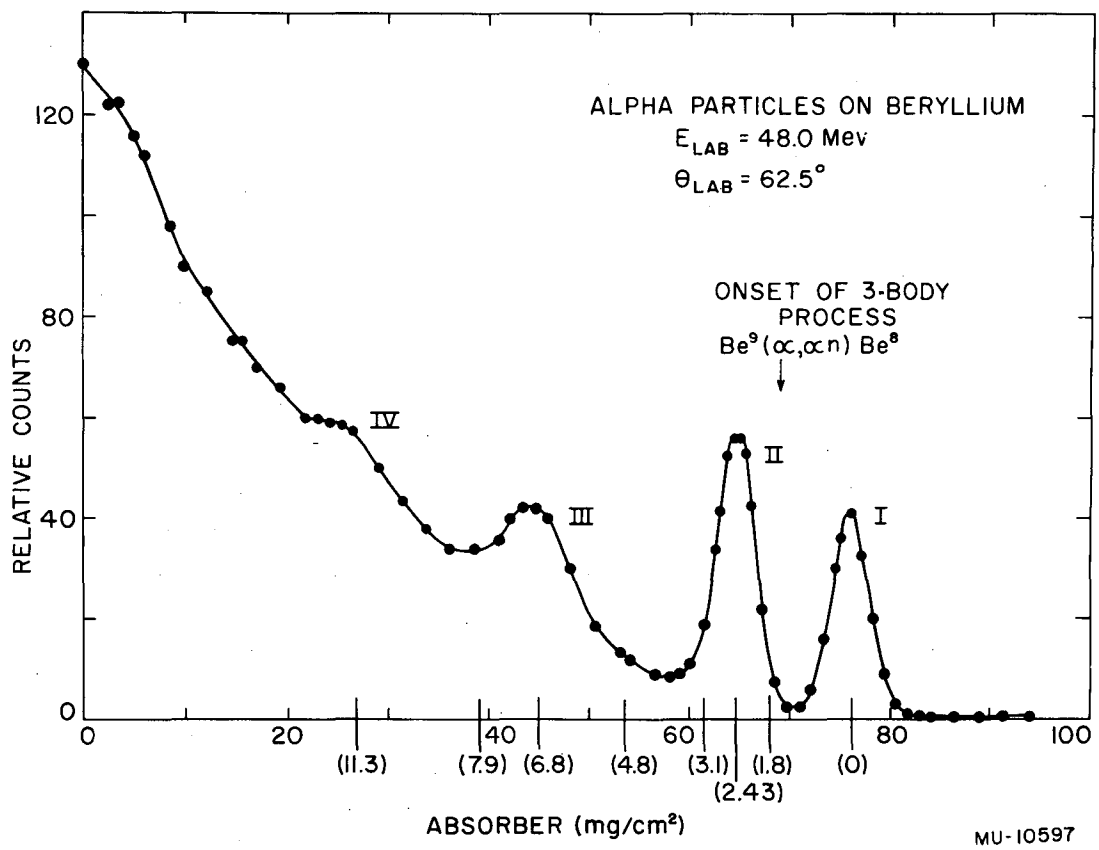

Fig. 15. Alpha-particle spectrum from beryllium bombarded with 48-Mev alpha particles. The short leaders along the abscissa indicate the expected positions of particle groups.

The spectral region in the vicinity of the elastic and 2.43-Mev inelastic peaks was studied in detail at some 35 angles from 7° to 90° in the laboratory frame. Measurements beyond 90°, requiring a reflection target, were impossible because of insufficient resolution. The difference in energy resolution between these alpha-particle measurements and the foregoing proton experiments is a consequence of the fact that 48-Mev alpha particles have a range only equal to that of the 12-Mev protons. Thus the separation in range of particle groups differing in energy by a given amount, i.e., 2.43 Mev, is considerably less for alpha particles. Figure 16 shows the differential elastic scattering cross section. The experimental points are represented by the solid circles. The solid curve was calculated from the usual Rutherford formula and the dashed curve obtained by division of the experimental values by the Rutherford cross section. The data are tabulated in Table IV. The differential cross section for inelastic scattering and the formation of the 2.43-Mev state is shown in Fig. 17 and listed in Table V. The total cross section for this reaction is 49.6 millibarns up to $\theta = 120^{\circ}$. If a flat angular dependence at greater angles is assumed, the total integrated cross section is 56 millibarns. The significance of the solid curve is discussed below.

As for the proton bombardments, a considerable continuum was observed. Since its beginning occurred close to the calculated onset of the three-body reaction $Be^9(\alpha, n\alpha')Be^8$, it was interpreted in that way. Because of the compression of the energy scale already noted, application of the analysis discussed in the Appendix may have included additional contributions due to the 4.8-Mev level and three-body reactions in which the Be^8 is left in an excited state. Figure 18 shows the data with these other reactions assumed to be negligible. The left-hand ordinate gives the differential cross section for the reaction $Be^9(\alpha, n\alpha')Be^8$, in which the scattered alpha particle retains most of the energy so that $0.90E_{\alpha'}^{max} \leq E_{\alpha'} \leq E_{\alpha'}^{max}$. The right-hand ordinate shows the differential cross section for any scattered alpha-particle energy, assuming the division of energy is statistical. The slight structure visible is probably not real, since it corresponds closely to that observed

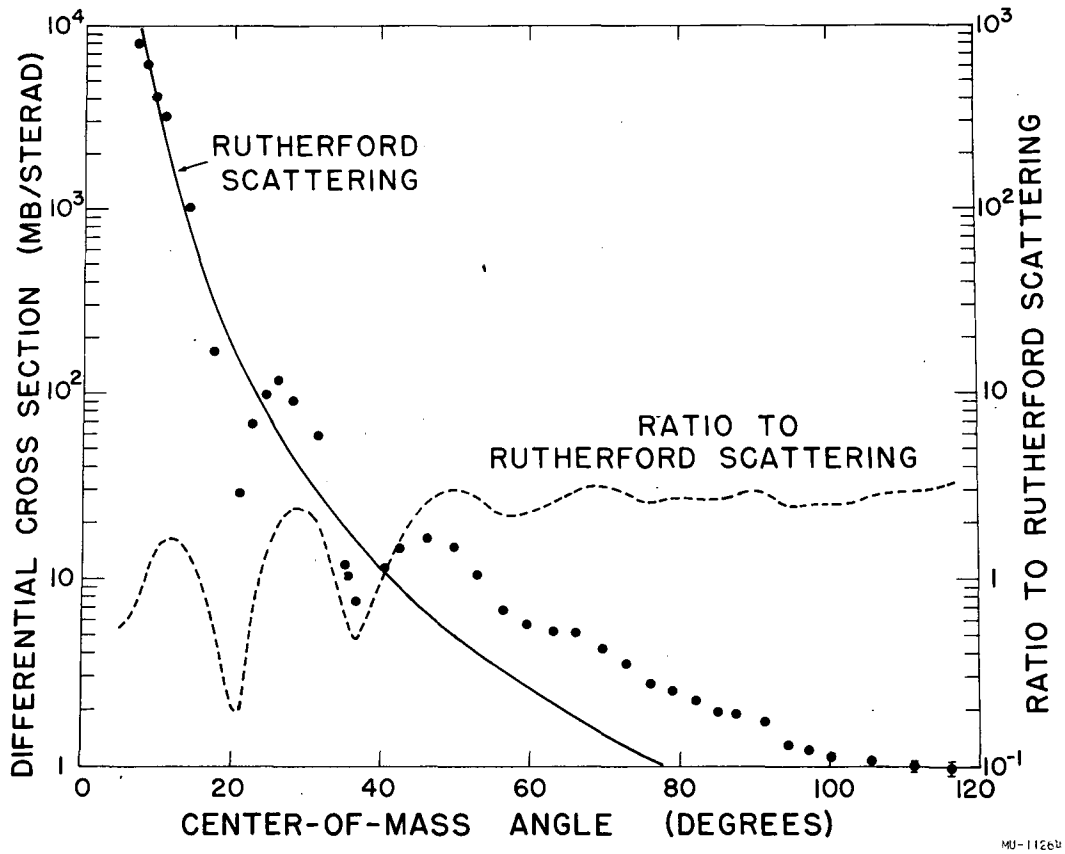

Fig. 16. The differential cross section for elastic alpha-particle scattering by beryllium at a laboratory energy of 48 Mev. Except where shown, experimental errors are smaller than the size of the points.

Table IV

Differential cross sections and their ratios to Rutherford cross sections for the elastic scattering of 48-Mev alpha particles by beryllium.

θ (degrees)	$d\sigma/d\Omega$ (mb/sterad)	$\frac{d\sigma}{d\Omega}\Big/\left(\frac{d\sigma}{d\Omega}\right)_c$	θ (degrees)	$d\sigma/d\Omega$ (mb/sterad)	$\frac{d\sigma}{d\Omega}\Big/\left(\frac{d\sigma}{d\Omega}\right)_c$
5.5	16800 ± 900	0.565 ± .030	53.0	10.5 ± .35	2.65 ± .09
7.0	7990 ± 260	0.709 ± .023	56.5	6.74 ± .22	2.16 ± .07
8.2	6130 ± 270	1.020 ± .045	59.7	5.70 ± .19	2.23 ± .07
9.5	4120 ± 130	1.238 ± .039	63.2	5.22 ± .18	2.51 ± .09
10.8	3200 ± 100	1.601 ± .050	66.2	5.16 ± .17	2.93 ± .10
13.9	1030 ± 20	1.410 ± .027	69.8	4.28 ± .16	2.93 ± .11
17.4	168 ± 5.5	0.560 ± .018	72.9	3.53 ± .12	2.81 ± .10
21.0	28.9 ± .70	0.204 ± .049	76.2	2.75 ± .09	2.54 ± .08
22.7	68.0 ± 2.0	0.650 ± .019	79.2	2.53 ± .09	2.66 ± .10
24.4	97.8 ± 3.4	1.244 ± .043	82.3	2.24 ± .08	2.68 ± .10
26.1	117.6 ± 4.1	1.950 ± .068	85.2	1.95 ± .07	2.61 ± .09
28.2	91.1 ± 2.1	2.045 ± .047	87.5	1.91 ± .07	2.78 ± .10
31.5	58.9 ± 2.1	2.035 ± .072	91.4	$1.73^{+.06}_{-.08}$	$2.90^{+.10}_{-.13}$
35.3	11.8 ± .4	0.636 ± .021	94.5	1.30 ± .05	2.41 ± .09
35.6	10.3 ± .4	0.572 ± .020	97.3	$1.24^{+.05}_{-.08}$	$2.51^{+.10}_{-.16}$
36.8	7.55 ± .26	0.477 ± .016	100.3	$1.13^{+.05}_{-.06}$	$2.50^{+.11}_{-.13}$
40.5	11.4 ± .4	1.043 ± .035	105.7	$1.07^{+.04}_{-.05}$	$2.75^{+.10}_{-.13}$
42.6	14.7 ± .2	1.634 ± .022	111.2	$0.99^{+.07}_{-.08}$	$2.92^{+.21}_{-.26}$
46.3	16.5 ± .55	2.52 ± .08	116.2	0.96 ± .11	3.18 ± .36
49.8	14.6 ± .5	2.92 ± .10			

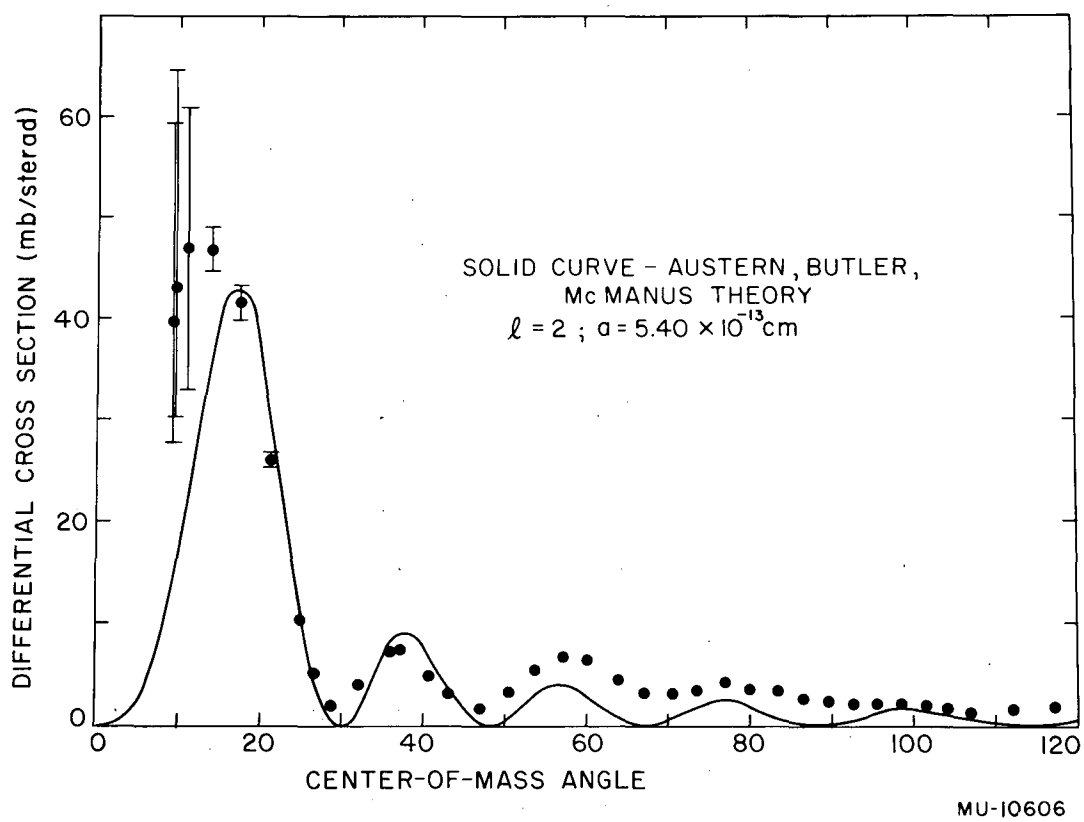

Fig. 17. The differential cross section for the formation of the 2.43-Mev state of beryllium by inelastic alpha-particle scattering. The laboratory energy was 48 Mev.

Table V

Differential cross sections for the inelastic scattering (2.43-Mev level) of 48-Mev alpha particles by beryllium.

θ (degrees)	$d\sigma/d\Omega$ (mb/sterad)	θ (degrees)	$d\sigma/d\Omega$ (mb/sterad)
9.3	43.1^{+22}_{-13}	60.2	6.37 ± .24
9.5	39.6^{+20}_{-12}	63.8	4.52 ± .18
10.9	46.9 ± 14	67.0	3.23 ± .13
13.9	46.8 ± 2.2	70.4	3.06 ± .13
17.4	41.5 ± 1.7	73.5	3.43 ± .13
21.2	26.0 ± .7	77.0	4.19 ± .15
24.8	10.3 ± .5	80.0	3.52 ± .13
26.6	5.12 ± .39	83.3	3.35 ± .13
28.7	2.06 ± .15	86.4	2.67 ± .07
32.0	4.05 ± .25	89.5	2.27 ± .06
35.8	7.25 ± .20	92.5	2.10 ± .09
37.1	7.42 ± .31	95.5	2.13 ± .09
40.7	4.78 ± .22	98.5	2.10 ± .09
43.0	3.24 ± .10	101.4	1.96 ± .10
46.8	1.69 ± .19	104.1	1.73 ± .09
50.3	3.38 ± .20	106.9	1.34 ± .07
53.7	5.46 ± .22	112.1	1.49 ± .10
57.1	6.71 ± .25	117.2	1.86 ± .15

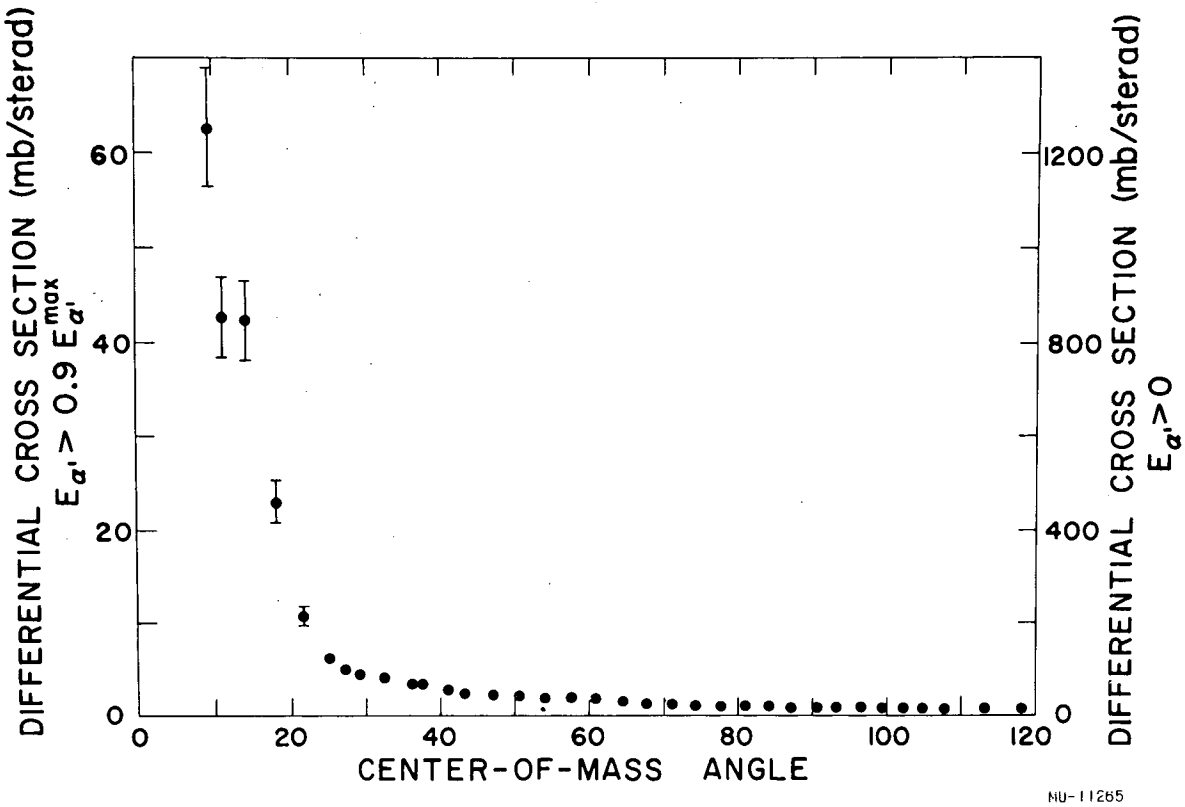

Fig. 18. The differential cross section for the reaction $Be^9(\alpha, n\alpha')Be^8$ at a laboratory energy of 48 Mev. The values on the left for $E_{\alpha'} > 0.9\ E_{\alpha'}^{max}$ were measured directly. Those on the right follow if the available energy is shared statistically among the products. Notice that the abscissa is the angle of scattering of the alpha particle.

in the cross section for the formation of the 2.43-Mev state. Thus it probably has its origin in slightly incorrect treatment of the experimental data.

C. Deuteron Bombardments

The same beryllium target was bombarded with 24-Mev deuterons and the charged-particle spectra studied as before. Because of the neutron hazard the time for these experiments was considerably curtailed. As a consequence, the data are not so complete nor so well established. The same neutron problem also, of course, compounded the difficulties in making the observations. At all angles substantial charged-particle backgrounds were observed, both with the target in and target out. Since a large part of this background was initiated by neutrons originating inside the cyclotron itself, its magnitude depended on the internal circulating beam as well as on the much smaller and measured external beam. This made reproducibility of results a problem.

A partial charged-particle spectrum was taken at one angle only, namely 25.6° in the laboratory frame. This is shown in Fig. 19. The relatively high-level background, even under the elastic Peak I, is apparent. The second peak shows the strongly excited 2.43-Mev level, while Peak V corresponds to the 6.8-Mev excited state. The slight bump, or more accurately the plateau, labeled IV is presumed to be due to the 4.8-Mev level. The origin of Peak III is not so clearly understood. As can be seen from the notation along the abscissa of the graph, its position corresponds closely to that projected for an inelastic deuteron group from the 3.1-Mev level in Be^9. However, it is also not far from the expected position of a possible triton group corresponding to a residual Be^8 nucleus in its 2.9-Mev excited state. Although at this angle no peak appears corresponding to ground-state tritons, a slight peak in just this position was visible at 30° though it was not evident at other angles. It seems possible, therefore, that the (d, t) reaction does occur, as has been found at other energies.[36] The peak labeled III

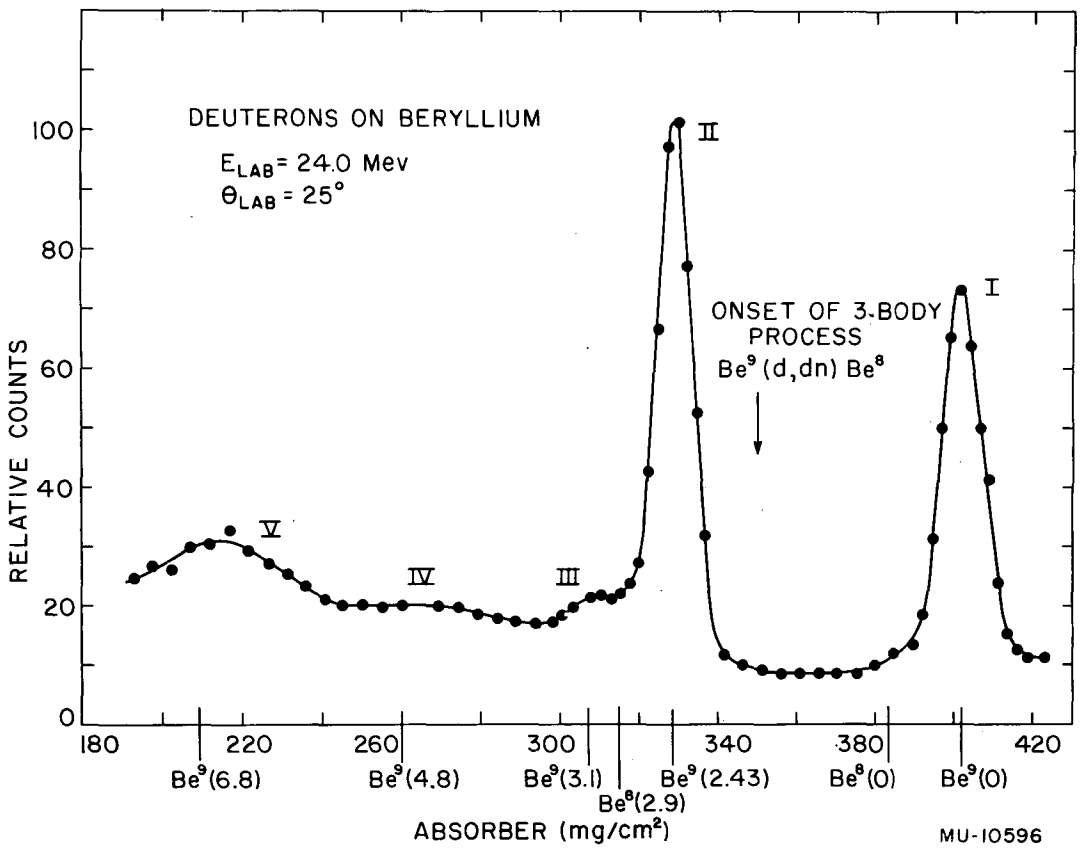

Fig. 19. Charged particles from the deuteron bombardment of beryllium. The short leaders along the abscissa indicate the expected positions of the peaks corresponding to the final nuclear states by which they are labeled.

was visible at 30°, 25°, and 15°. If it were a triton group, however, it might have been expected to be less prominent than the ground-state group. For this reason, interpretation as a deuteron group and evidence for the 3.1-Mev level are more likely. It was not possible to confirm this identification by discrimination in Chamber 1 of the detector owing, firstly, to the weakness of the group and, secondly, to the background consisting mainly of protons.

A weak 1.8-Mev "level" would doubtless not have been visible, owing to this same proton background. In fact, as can be seen from the figure, the onset of the (d, nd') reaction is masked by the same effect. Not shown on Fig. 19 are points taken with very thick absorbers in an effort to identify possible proton groups from the reaction $Be^{9}(d, p)Be^{10}$. Evidence for such groups was not found. The background that persisted even at these absorber values (950 mg/cm^{2} for ~27.5-Mev protons) might well, however, have masked weak monoenergetic particle groups.

The elastic differential cross section was measured, partly by differential scanning, partly by integral means, at laboratory angles ranging from 7° to 167°. These results are listed in Table VI and shown by the solid circles of Fig. 20. The solid curve represents classical Rutherford scattering and the dashed curve indicates the ratio to Rutherford scattering calculated from the observed data.

The peak corresponding to the 2.43-Mev state was scanned at laboratory angles ranging from 15° to 150°. The resulting inelastic cross section is shown in Fig. 21, where the points are the experimental data. The curve, derived from theory, is discussed below. A tabulation of the data may be found in Table VII. Measurement of the cross section at more forward angles was impossible, because of the high-level background and the large elastic cross section. This swamping may be taken as evidence that the inelastic cross section does not increase for $\theta < 15^{\circ}$. The total integrated cross section, which is rather insensitive to the behavior at small angles, is 44.0 millibarns.

Analysis of the continuum was not possible in this case as it was for the proton and alpha-particle bombardments. In addition to the neutron-initiated background, other multibody processes $Be^{9}(d, pn)Be^{9}$ and $Be^{9}(d, p2n)Be^{8}$ can compete with the analagous $Be^{9}(d, nd')Be^{8}$ reaction.

Table VI

Differential cross sections and their ratios to Rutherford scattering for the elastic scattering of 24-Mev deuterons by beryllium

θ (degrees)	$d\sigma/d\Omega$ (mb/sterad)	$\left(\frac{d\sigma}{d\Omega}\right)/\left(\frac{d\sigma}{d\Omega}\right)_c$	θ (degrees)	$d\sigma/d\Omega$ (mb/sterad)	$\left(\frac{d\sigma}{d\Omega}\right)/\left(\frac{d\sigma}{d\Omega}\right)_c$
9.3	2900 ± 80	1.55 ± .04	77.4	5.05 ± .27	9.54 ± .51
12.9	1650 ± 70	3.27 ± .14	82.8	4.59 ± .25	10.82 ± .59
19.0	613 ± 20	5.63 ± .18	93.3	2.68 ± .15	9.25 ± .52
22.2	317 ± 10	5.39 ± .17	102.3	1.57 ± .10	7.13 ± .45
25.1	150 ± 10	4.11 ± .27	103.5	1.47 ± .09	6.90 ± .42
28.1	38.8 ± 2.3	1.67 ± .10	112.1	1.13 ± .08	6.60 ± .47
31.1	9.12 ± .50	0.582 ± .032	121.5	1.12 ± .08	8.02 ± .57
34.1	7.26 ± 1.3	0.66 ± .12	130.6	1.07 ± .07	9.02 ± .59
37.1	12.3 ± 0.4	1.56 ± .05	139.4	0.83 ± .06	7.94 ± .57
43.1	26.6 ± 1.3	6.00 ± .29	145.7	0.56 ± .05	5.76 ± .51
49.0	22.5 ± 0.7	8.21 ± .26	151.9	0.43 ± .04	4.71 ± .44
54.8	14.2 ± 0.4	7.86 ± .24	157.9	0.49 ± .05	5.64 ± .57
60.6	7.29 ± 0.38	5.85 ± .30	163.9	0.71 ± .06	8.45 ± .71
66.2	4.15 ± 0.44	4.56 ± .48	169.8	0.95 ± .13	11.6 ± 1.6
71.8	5.04 ± 0.28	7.36 ± .41			

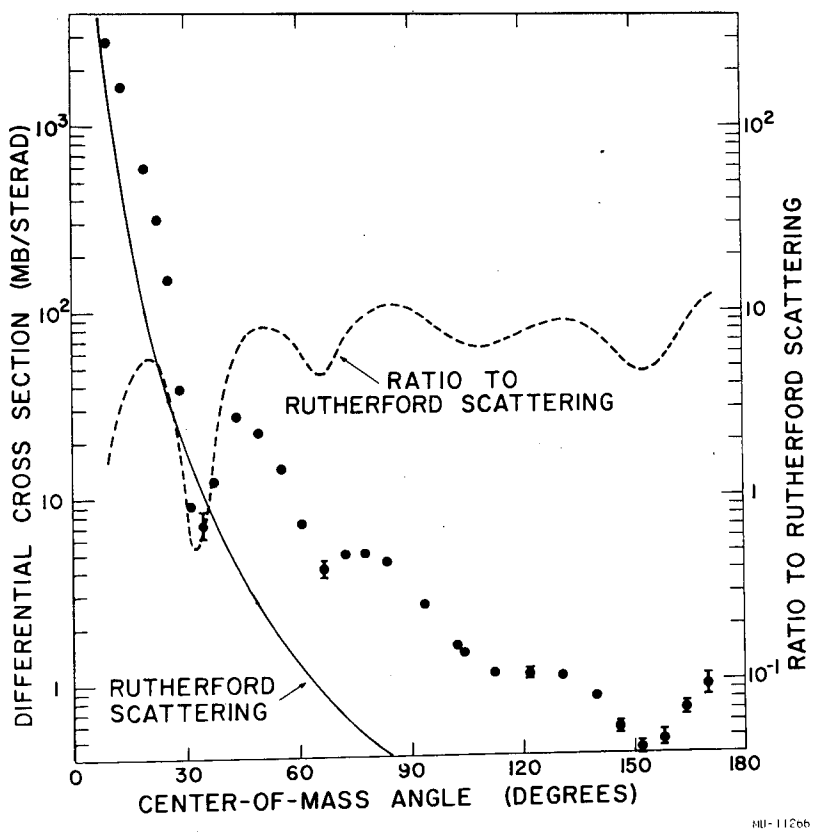

Fig. 20. The differential cross section for elastic deuteron scattering by beryllium at a laboratory energy of 24 Mev. Except where shown, experimental errors are smaller than the size of the points.

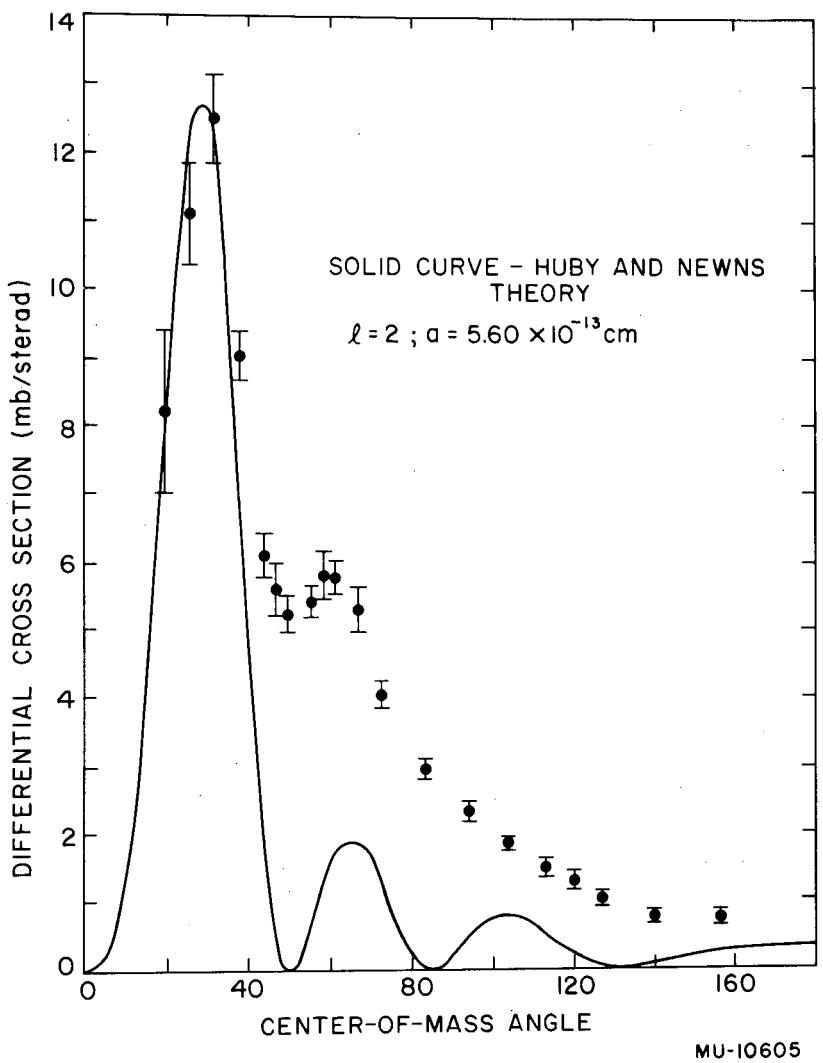

Fig. 21. The differential cross section for the formation of the 2.43-Mev state of beryllium by inelastic deuteron scattering. The laboratory energy was 24 Mev.

Table VII

Differential cross sections for the inelastic scattering (2.43-Mev level) of 24-Mev deuterons by beryllium.

θ (degrees)	$d\sigma/d\Omega$ (mb/sterad)
19.3	8.19 ± 1.2
25.3	11.08 ± .74
31.4	12.5 ± .65
37.6	9.00 ± .36
43.6	6.08 ± .33
46.6	5.57 ± .39
49.5	5.21 ± .27
55.4	5.39 ± .24
58.3	5.78 ± .36
61.2	5.75 ± .24
66.9	5.27 ± .33
72.6	4.02 ± .21
83.5	2.93 ± .16
94.2	2.31 ± .15
103.8	1.83 ± .10
113.0	1.48 ± .15
120.1	1.28 ± .14
126.9	1.02 ± .12
140.0	0.75 ± .11
156.4	0.74 ± .12

V. DISCUSSION

The data have been reviewed in order according to the initiating projectile. In this section data of the same type are discussed together in order to emphasize similarities and differences. Accordingly, there are six subheadings.

A. Elastic Scattering

The scattering of a charged particle by a point charge has long been understood, the differential cross section being given by the Rutherford formula

$$\left(\frac{d\sigma}{d\Omega}\right)_c = \left(\frac{Z\,z\,e^2}{4\,E}\right)^2 \csc^4 \frac{\theta}{2},$$

where Ze is the charge of the scattering center,

ze is the charge of the scattered particle,

E is the center-of-mass approach energy, and

θ is the center-of-mass angle of scattering.

The derivation of this formula requires only the assumption that the force between the particles is Zze^2/r^2.

The elastic scattering of protons, deuterons, and alpha particles from a nucleus deviates from this expression for two reasons:

(a) Because of the finite size of the charge distribution in the nucleus, the $1/r^2$-dependence of the Coulomb force breaks down if the bombarding particle penetrates the nucleus.

(b) Non-Coulombic forces, namely nucleon-nucleon interaction, are present. Since these forces are of short range, deviations from the Rutherford formula are to be expected once again only if the bombarding particle comes close to the nucleus.

A study of these deviations from pure Coulomb scattering can therefore shed light on the size of the nucleus and on the nature of nuclear forces.

The results of dividing the observed data by the Rutherford cross sections are given in Figs. 11, 16, and 20 and in Tables I, IV, and VI. Interference effects are prominent. Except at small angles, corresponding to large distances of closest approach, absolute values of the scattering cross sections exceed those computed from the formula.

One of the simplest ways to interpret elastic scattering data is to assume[37] that the nucleus is opaque to particles which in a classical picture would hit the nucleus. Particles that "miss" the nucleus are assumed to proceed without interaction (other than Coulomb, that is). Such a picture is, of course, the more valid the greater the observed ratio to Rutherford scattering. Under these assumptions the problem is reduced to that of Fraunhofer diffraction* from a circular disk and the angular distribution is proportional to

$$\left[\frac{J_1\left(2kR\sin\frac{\theta}{2}\right)}{2kR\sin\frac{\theta}{2}}\right]^2,$$

where $J_1(x)$ is the regular Bessel function of first order,

- k is the center-of-mass wave number of the incident particle,
- θ is the center-of-mass angle of scattering, and
- R is the radius of interaction (i.e., the sum of the effective radii of the nucleus and incident particle).

Roughly speaking, successive maxima or minima of this function are separated by π. This leads to the criterion that for adjacent maxima or minima $2kR\,\Delta\sin\frac{\theta}{2} = \pi$. Table VIII lists the angles at which maxima or minima were found and the values of R calculated from the above formula for each of the three elastic scattering processes observed. It is apparent that such a rough explanation of the origin of the interference effects is not completely adequate. The positions of the maxima and minima and their heights and depths do not follow such a simple law.

---

* In a more exact calculation, where it is remembered that the nucleus is spherical, not circular, the expression obtained is $\left[\frac{j_1\left(2kR\sin\frac{\theta}{2}\right)}{2kR\sin\frac{\theta}{2}}\right]^2$. Since the maxima and minima of this quantity are similarly separated by approximately π, the determination of the interaction radii is unchanged.

Table VIII

Interaction radii obtained by diffraction analysis of elastic scattering

Incident Particle	Position of feature (degrees)		$R \times 10^{13}$ (cm)	Mean $R \times 10^{13}$ (cm)
	Maxima	Minima		
p		8 ± 1		
			4.4 ± 0.1	
		72 ± 1		
				4.6 ± 0.1
	45 ± 2			
			4.8 ± 0.2	
	117 ± 2			
α	12.2 ± 1.0			
			5.2 ± 0.4	
	29.0 ± 1.0			
			4.4 ± 0.3	
	49.5 ± 1.0			
			5.3 ± 0.4	
	68 ± 1			
			5.0 ± 0.4	
	90 ± 2			
				4.9 ± 0.2
		20.0 ± 0.5		
			5.2 ± 0.2	
		37.0 ± 0.5		
			4.5 ± 0.3	
		57.5 ± 1		
			4.6 ± 0.4	
		80 ± 2		
d	20.5 ± 1.0			
			5.0 ± 0.2	
	51 ± 1			
			5.3 ± 0.3	
	84 ± 2			
			5.2 ± 0.3	
	131 ± 3			
				5.0 ± 0.1
		32.5 ± 1.0		
			4.8 ± 0.2	
		65.5 ± 1.0		
			4.6 ± 0.2	
		109 ± 2		
			4.9 ± 0.2	
		152 ± 1		

A single value $r_{Be} = 3.4 \times 10^{-13} = 1.64\ A^{1/3} \times 10^{-13}$ cm is obtained from these interaction radii if it is assumed that $r_p = 1.2 \times 10^{-13}$ cm, $r_\alpha = 1.5 \times 10^{-13}$ cm, and $r_d = 1.6 \times 10^{-13}$ cm. The proton radius is quite reasonable. While the free-space radius of the alpha particle[38] is no doubt nearer 2.3×10^{-13} cm, a smaller value is in line with that generally found when the alpha particle is in the Coulomb field of the nucleus. The electrostatic repulsive force exceeds the internuclear attractive force until there is considerable overlap. Blatt and Weisskopf,[39] for example, choose the effective radius of the alpha particle to be 1.2×10^{-13} cm. Elastic scattering experiments by Igo, Wegner, and Eisberg[40] at 40 Mev yielded an effective alpha-particle radius of $(1.60 \pm .23) \times 10^{-13}$ cm. The fact that the deuteron radius[41] above is considerably smaller than the so-called "radius of the deuteron," 4.4×10^{-13} cm, is not surprising. If a collision took place at a time when the neutron and proton were widely separated and outside the range of their forces, scattering of the deuteron as a whole would not be expected. An effective deuteron radius less than the range of forces,[41] 2.1×10^{-13} cm, should be anticipated. If the beryllium radius seems large, recall that because of the very low binding energy in beryllium a large amount of the wave function is able to leak out of the potential well. Radii derived from mirror nucleus considerations or from the scattering of electrons are normal, since such experiments measure the charge distribution only.

The above analysis has been based on a rather rough postulate, namely total absorption of particles incident on the nucleus itself. For a nucleus as small as beryllium this is hardly justified. Furthermore, the model does not allow for a fuzzy nuclear edge, a region of smooth variation from no nuclear matter to the maximum nuclear density. A model that seeks to be more realistic is due to Woods and Saxon.[42] These authors assume a four-parameter nucleon-nucleus interaction of the form

$$V_N(r) = -\frac{V + iW}{1 + \exp\left[(r - R_0)/a\right]}.$$

They give the Coulomb force the correct form for a homogeneously charged sphere of radius R_0, namely

$$V_c(r) = \frac{Ze^2}{2R_0}\left(3 - \frac{r^2}{R_0^2}\right), \quad r \leq R_0$$

$$= \frac{Ze^2}{r}, \quad r \geq R_0.$$

Here V and W are the real and imaginary parts of the nuclear potential, which is given the shape of a rounded square well by the form factor in the denominator. The term R_0 is the "radius" of the well, while a is a measure of the diffuseness of the edge. Different charge and nuclear-potential radii make little difference in the calculated scattering distributions.

This model has proved to be quite successful in the analysis[43] of the scattering of 14-Mev neutrons and 5.25-Mev, 17-Mev, and 31.5-Mev protons. The calculation involves the systematic variation of the four parameters, with the aid of an electronic computer, until best fit for an elastic cross section is obtained. Such fits are usually fairly good out to angles of the order of 120°. The noteworthy fact about this model is that the values of the parameters so found are virtually independent of A (except for the expected $A^{1/3}$ dependence of R_0), and show a smooth variation with nucleon bombarding energy. There seem to be no essential differences between the values found for neutrons and protons. The values found for R_0 and a are $(1.33 \pm .03)\ A^{1/3} \times 10^{-13}$cm and $(0.49 \pm .02) \times 10^{-13}$ cm respectively. These parameters are energy-independent. The values of V and W are listed in Table IX.

Table IX

Energy dependence of the diffuse-surface optical model parameters

Nucleon energy (Mev)	Real potential (Mev)	Imaginary potential (Mev)
5.25	52.5	0.9
14 (neutrons)	~47	~8
17	47 ± 1	8.5 ± 0.5
31.5	36 ± 1	15.5 ± 0.5

Calculations similar to the above have not yet been carried out on the data presented here. The proton data have been incorporated with the results of a wide survey of proton elastic scattering,[44] which is being carried out at this laboratory. Arrangements have been made to have this complete survey analyzed in terms of the optical model. Unfortunately this analysis is awaiting further measurements on a few more elements. It is hoped that a similar survey and analysis will soon be undertaken for elastic deuteron and alpha-particle scattering. In the latter case, data available at 48 Mev already include the elements C, and Mg,[33] and Ag, Au, and Pb[32] in addition to Be reported here.

B. The (p, d) Reaction

The theory of (d, p) reactions at intermediate energies was first treated successfully by Butler.[25] Since that time the original assumptions of no Coulomb effects and of no nuclear interaction between the proton and the nucleus have been relaxed.[45] Unfortunately these more realistic theories involve very lengthy numerical calculations.

Butler's formula for the differential cross section at angle θ may be written[46]

$$\frac{d\sigma}{d\Omega} \sim \left[G\left(\left|\vec{k}_p - \frac{\vec{k}_d}{2}\right|\right)\right]^2 \sum_{\ell} \left\{A_\ell j_\ell (kR_0) + B_\ell \left(\frac{kR_0}{2\ell+1}\right) \left[\ell j_{\ell-1}(kR_0) - (\ell+1) j_{\ell+1}(kR_0)\right]\right\}^2,$$

where $G\left(\left|\vec{k}_p - \frac{\vec{k}_d}{2}\right|\right)$ is the probability of finding the proton within the deuteron with momentum $\hbar\vec{k}_p$ instead of the mean momentum $(1/2)\,\hbar\vec{k}_d$,

$k = |\vec{k}_d - \vec{k}_p| = (k_d - k_p)^2 + 4k_d k_p \sin^2\frac{\theta}{2}$,

$\hbar\vec{k}_d$ is the momentum of the incident deuteron,

$\hbar\vec{k}_p$ is the momentum of the observed proton,

R_0 is the radius of interaction,

$\ell\hbar$ is the angular momentum of the captured neutron,

A_ℓ and B_ℓ are angularly independent constants, and

j_ℓ is the regular spherical Bessel function of order ℓ.

The terms within the summation give essentially the probability that the neutron traveling with momentum $\hbar\vec{k}_d - \hbar\vec{k}_p$ be found at the surface of the nucleus in a state of angular momentum ℓ with respect to that nucleus. The second term, which is simply the derivative of the spherical Bessel function, arises from the requirement that in the matching of wave functions at a boundary both magnitudes and derivatives must be equal. Conservation of angular momentum and parity leads to the selection rules

$$J_i + J_f + \frac{1}{2} \geq \ell \geq \left| \vec{J}_i + \vec{J}_f + \vec{\frac{1}{2}} \right|_{min} \text{ and } \pi_f \pi_i = (-1)^{\ell} .$$

Generally speaking, the lowest allowed ℓ value predominates. Thus the position of the first maximum of the differential cross section permits a determination of the final-state properties so far as the selection rules allow.

By detailed balance, all of the above considerations apply equally well to deuteron pickup reactions. Figure 13 shows the theoretical cross section (normalized for best fit in the region form 10° to 30°) for the reaction $Be^9(p,d)Be^8$ at 12 Mev. The values of the parameters used are $\ell = 1$ and $R_0 = 4.50 \times 10^{-13}$ cm. Poorer fits of the observed shape for other ℓ values required inordinately small or large radii of interaction. The value $\ell = 1$ is in agreement with the already known initial and final spins and parities. Of more interest is the value of R_0. It compares favorably with that found from elastic proton scattering. Further remarks are deferred to a later subsection.

C. The 2.43-Mev State

The differential cross sections for the three inelastic scattering reactions (p, p'), (α, α'), and (d, d') leading to the 2.43-Mev excited state of Be^9 have been determined. All three curves show pronounced maxima in or near the forward direction and were analyzed by using direct-interaction theories.

Because of the unlikelihood of the emission of a deuteron from a compound nucleus the (d, d') reaction probably occurs predominantly by surface interaction. According to Huby and Newns,[47] under such an assumption the differential cross section will have an angular dependence given by

$$\frac{d\sigma}{d\Omega} \sim \left[\frac{4\alpha}{G} \tan^{-1} \frac{G}{4\alpha}\right]^2 \sum_{\ell} A_{\ell}^2 \; j_{\ell}^2 \; (Ga),$$

where G is the change in momentum of the deuteron during the interaction and is given by the quantity $\left[(k-k')^2 + 4kk' \sin^2 \frac{\theta}{2}\right]^{1/2}$,

k is center-of-mass wave number of the incident deuteron,

k' is the center-of-mass wave number of the scattered deuteron,

θ is the center-of-mass scattering angle,

α is a constant of the deuteron wave function, which was taken as $\frac{1}{r} e^{-\alpha r}$ in the region outside the potential well,

a is the interaction radius,

A_{ℓ} are nuclear matrix elements and are independent of angle,

$j_{\ell}(x)$ is the regular spherical Bessel function of order ℓ, and

$\ell\hbar$ is the orbital angular momentum transferred to the nucleus during the collision.

Since the form factor in the square brackets decreases monotonically with increasing angle, the peaks of higher ℓ values are suppressed. Similarity to the stripping-reaction distribution is apparent.

Selection rules* that apply in this process are

$$J_i + J_f \leq \ell \leq \left|\vec{J}_i + \vec{J}_f\right|_{min} \quad \text{and} \quad \pi_i \pi_f = (-1)^{\ell}.$$

The possibility of spin flip is not present, since the flip of only one member of the deuteron would result in its breakup and consequent loss from the (d, d') reaction. The flip of both nucleons can occur

---

* These differ from the selection rules of Huby and Newns for the reason suggested above. Experimental results[48] in cases where initial and final spins are known do not require the extra freedom in angular-momentum transfer granted by spin flip.

only in higher order as long as one confines the discussion to two-body forces. Multibody forces are likely to be important only for closer collisions. Such collisions would tend once again to break up the loosely bound deuteron.

Figure 21 shows the theoretical curve for $\ell = 2$ and $a = 5.60 \times 10^{-13}$ cm. The first peak fits the experimental data well. The second, while agreeing in position with the second experimental peak, is several times too small. The addition of an equal amount of the term in $\ell = 4$ (not shown) gives close agreement with experiment out to an angle of 70°. Whether such close agreement is to be expected from the theory is not clear. Certainly, in this type of reaction, compound-nucleus effects should be minimized. If $a = 3.40 \times 10^{-13}$ cm is used, the theoretical curve for $\ell = 1$ can reproduce the first maximum, but the second then falls at $\theta = 95^{\circ}$. Such a small value for the interaction radius $a = r_0 A^{1/3} + r_d$ makes this interpretation highly unlikely.

Taking $\ell = 2$* and the spin-parity of the Be^9 ground state, we find that application of the selection rules leads to the assignment 1/2, 3/2, 5/2, or 7/2, all odd parity, for the 2.43-Mev state. The absence of an $\ell = 0$ fit (if allowed, this transition should have dominated) eliminates the possibility of 3/2.

Austern, Butler, and McManus[26] developed, and more recently Satchler[49] has reformulated, a theory of direct interaction applicable to (n, p), (n, n'), and (p, p') reactions. The differential cross section has the form

$$\frac{d\sigma}{d\Omega} \sim \sum_{\ell} A_{\ell}^{2} \; j_{\ell}^{2} \; (Ga),$$

where the quantities are the same (except for the obvious transliteration) as those defined above. Of course the matrix elements involved will have different values. No form factor is present, since the incident

---

* For $\ell = 2$ and $\ell = 4$ combined, the final-state assignment is 5/2 or 7/2, both odd parity.

and scattered particles do not have an internal structure; that is, all of the particle takes part in the collision. While the original authors required the assumption that nucleon-nucleon cross sections are isotropic and independent of energy, the only basic assumption of the reformulation is that of zero-range forces. Recently, Vaughn[33] has found that this theory correctly predicts the positions of the sharp maxima and minima that were observed in the differential cross sections for the inelastic scattering of alpha particles from magnesium and carbon. Because its components are so strongly bound together, the alpha particle probably acts as much like a billiard ball at moderate energies as any single nucleon does.

Application of this theory to the inelastic (2.43-Mev state) alpha-particle scattering from beryllium is shown in Fig. 17. The curve has been drawn for $\ell = 2$ and $a = 5.40 \times 10^{-13}$ cm. In this case the value of the interaction radius was chosen to yield the best fit of the positions of the minima at 29° and 47°. Except for the measurements for $\theta < 15^{\circ}$, which are subject to large errors, the agreement between theory and experiment is remarkable. The best fit for $\ell = 1$ requires $a = 4.63 \times 10^{-13}$ cm. While this value of the interaction radius could be accepted, this theoretical curve fits the width of the first maximum very poorly and places the higher-order maxima and minima at too large angles.

Since the alpha particle has no intrinsic spin, the selection rules applicable for this case are the same as those set down above, namely,

$$J_i + J_f \geq \ell \geq \left| \vec{J}_i + \vec{J}_f \right|_{min} \quad \text{and} \quad \Pi_i \Pi_f = (-1)^{\ell}.$$

For $\ell = 2$ and $J_i = 3/2$ -, the spin assignment for the 2.43-Mev state is again 1/2, 5/2, or 7/2, all odd parity. The possibility of 3/2 is eliminated because of the absence of a predominating $\ell = 0$ distribution.

Figure 12 shows the observed results for the formation of this same level by inelastic proton scattering. Their interpretation by direct interaction theory is not immediately apparent. The greatly reduced ratio of the maximum to the minimum cross section indicates that a not negligible amount of the excitation takes place via compound-nucleus

formation. In that regard these results are in agreement with other inelastic proton-scattering data[50] at the same laboratory energy. The data[16] for the inelastic scattering of 31.3-Mev protons from beryllium strongly suggest that direct interaction accounts for most of the cross section at that energy. Consequently, an explanation for the 12-Mev data presented here will be sought in a combination of the compound-nucleus and direct-interaction theories. In fact, there is no fixed line of demarcation between a fringe interaction and a process in which the initial nucleon is absorbed into a compound nucleus that reaches thermal equilibrium before decay. Nevertheless, for want of any other more realistic theory, the differential cross section is written

$$\frac{d\sigma}{d\Omega} = \left(\frac{d\sigma}{d\Omega}\right)_{CN} + \left(\frac{d\sigma}{d\Omega}\right)_{ABM} .$$

No interference term is present, since fringe interaction is instantaneous, while re-emission by the compound nucleus follows the initial absorption only after a lapse of time that is long compared with the time for a nucleon to cross the nucleus.

According to compound-nucleus theory, if the reaction proceeds through only one level of the intermediate state the cross section is necessarily symmetric about 90° in the center-of-mass frame. A similar result is obtained if a statistically large number of compound states is involved so that the phases of the various contributing waves average out. If only a few compound levels contribute, not all with the same parity, then this condition about symmetry is removed.

For 12-Mev protons incident on Be^{9} the compound nucleus B^{10} would have an excitation of 17.4 Mev. Unfortunately no data are available at these excitations for B^{10}. As a crude estimate, the number of states presently known in C^{12} at this level of excitation is about three levels per Mev. Presumably a nucleus like B^{10}, which does not have the possibility of alpha-particle substructure, may have, say, five times as many. Thus the level separation may be 50 or 100 kev. Application of the statistical level-density formula

$$\omega(E) = Ce^{2\sqrt{aE}}$$

is definitely questionable. Nevertheless, using extrapolated values of the constants for odd-A nuclei, one finds a level density of the same magnitude.

Information regarding level widths is also lacking. From the statistical theory, we have

$\Gamma_i \approx T_{\ell i} \frac{D}{2\pi}$, where $T_{\ell i}$ is the transmission factor for a particle i with angular momentum ℓ crossing the nuclear boundary, and D is the average level spacing.

For energies as high above the threshold for neutron emission as are here being considered, $T_{\ell n} \sim 1$ for $\ell \leq 2$ and drops off sharply for higher angular momenta. The partial widths for charged-particle emission are small by comparison. The total level widths are therefore perhaps of the order of the level spacing. Consequently, the coherent excitation of a large number of states is unquestionably impossible. On the other hand, the excitation of a single level is by no means assured. There is a reasonable possibility, therefore, that the compound-nucleus cross section, under these conditions, is not symmetric with respect to 90°.

In a classical picture partial waves with $\ell > 2$ cannot strike the nucleus. Since the combined Coulomb-centrifugal barrier height exceeds the incident proton energy for $\ell \geq 2$, one might expect the major part of the absorption to be s and p waves only. By a theorem on the angular distributions of nuclear reactions,[51] if a cross section of the form $\frac{d\sigma}{d\Omega} = \sum_n A_n \cos^n\theta$ is assumed, the highest value of n allowed would be 2 (4 if d waves take part). A rough fit of the experimental curve can be made by using terms up to $\cos^4\theta$. There is a possibility, therefore, that the entire observed cross section is due to compound-nucleus formation.

On the other hand, the shape of the cross section for $\theta > 90^{\circ}$ strongly suggests a form no more complicated than

$$\frac{d\sigma}{d\Omega} = A_0 + A_2 \cos^2\theta.$$

The dot-dash curve of Fig. 12 is plotted for $A_0 = 6.4$ and $A_2 = -2.7$. On this basis the cross section still to be accounted for is strongly peaked in the forward direction.

A fit of this residual cross section with a single ℓ value of the ABM theory is impossible. The forward peak is too broad to be fitted with $\ell = 1$. Furthermore, to be consistent with the results derived from the deuteron and alpha-particle scattering, only even ℓ values are allowable. Since the proton has spin 1/2, which is free to be flipped during interaction, the ABM theory for inelastic proton scattering has two selection rules,

$$J_i + J_f + 1 \geq \ell \geq \left| \vec{J}_i + \vec{J}_f + \vec{1} \right|_{min},$$

and

$$J_i + J_f \geq \ell \geq \left| \vec{J}_i + \vec{J}_f \right|_{min},$$

according to whether spin flip occurs or does not. The parity rule remains the same in both cases, $\Pi_i \Pi_f = (-1)^\ell$. In the discussion of the two other direct interactions considered it was stated that the $\ell = 0$ transition would dominate if permitted. The possibility presents itself here, however, that a transition requiring spin flip of the incident particle may be considerably suppressed. Thus an $\ell = 0$ transition with spin flip could be comparable in magnitude to or weaker than a higher-order transition (here $\ell = 2$) not involving spin flip.

Before we attempt to fit the residual proton cross section using a mixture of $\ell = 0$ and $\ell = 2$ components, we present some remarks that permit an estimate of a most probable radius of interaction. Elastic α-particle scattering led to a value for the interaction radius of 4.9×10^{-13} cm. On the other hand the best fit of the inelastic data yielded 5.4×10^{-13} cm. Values obtained from the deuteron data were 5.0×10^{-13} cm and 5.6×10^{-13} cm for the elastic and inelastic scattering respectively. Conclusive evidence* that these differences are real is still lacking. The trend towards larger radii for inelastic events is,

---

* The alpha-particle data of Vaughn[33] show the same effect.

however, understandable, because these presumably result from collisions between the incident particle and the mere "tail" of the nuclear wave function. The diffraction pattern of elastic scattering, on the other hand, has its origin in the loss from the incident beam of those particles absorbed into a compound nucleus. On this basis, then, since the interaction radius for elastic proton scattering was 4.6×10^{-13} cm, an inelastic value near 5.0×10^{-13} cm might be expected.

The curves shown in Fig. 12 have been calculated from the ABM theory for $\ell = 0$ and $\ell = 2$ with interaction radii 4.5×10^{-13} and 5.5×10^{-13} cm. While no quantitative fit is possible, it would appear that an $\ell = 0$ contribution is present. In a more realistic model[26] of surface interaction, in which that part of the incident wave which strikes the core of the nucleus is absorbed (and therefore lost to the direct interaction process), the forward minima of $\ell > 0$ transitions are more shallow. Since the theory loses its closed form under such conditions, exact calculations were not attempted. There is no doubt that such an alteration could permit agreement between the observed differential cross section and the combined compound nucleus plus $\ell = 0$ direct-interaction plus $\ell = 2$ direct-interaction theory. Of course the number of disposable parameters is large.

In summary, the inelastic proton cross section can probably be explained

(a) as entirely due to compound-nucleus formation, provided at least two levels with different parity and $J \geq 2$ are involved, or

(b) as partially due to a more simple compound-nucleus distribution along with a mixed direct-interaction process in which the angular momentum absorbed from the scattered protons is both 0 and 2.

If the second alternative is correct, application of the selection rules implies that $J_f = 1/2$, $3/2$, or $5/2$, all with odd parity.

As pointed out in an earlier section, measurements on the reaction $B^{10}(n, d)Be^{9*}$ by Ribe and Seagrave[20] indicated that the spin-parity of the 2.43-Mev state is 3/2, 5/2, 7/2, or 9/2, all odd parity. The only assignment consistent with these results and the alpha-particle, deuteron, and proton data herein reported is 5/2 -. (If the proton data are explained

wholly by compound-nucleus formation, then 7/2 - is also possible.) The most recent calculations[3] of the intermediate coupling model for beryllium do, indeed, predict that result.

The interpretation of the 31.3-Mev inelastic proton-scattering data[16] can be altered to agree with this assignment. The authors obtained a best fit with the ABM theory for $\ell = 1$ and $a = 2.80 \times 10^{-13}$ cm. A poorer fit, they report, is possible for $\ell = 2$ and $a = 4.15 \times 10^{-13}$ cm. By virtue of their semilogarithmic plot of the data, the values of the parameters chosen were unduly influenced by near minimum cross sections. When allowance is made for the reduction of the depth of the forward minimum due to the absorption of part of the incident wave and for a weak $\ell = 0$ transition, a reasonable fit of their data is possible for $\ell = 2$ and a radius of interaction as large as 4.5×10^{-13} cm. Such a value of a would be in better agreement with the effective radius, 4.0×10^{-13} cm, which they found from elastic scattering. Of course, $\ell = 2$ allows the assignment 5/2 - .

As stated, the assignment for this level is in accord with the intermediate-coupling shell-model prediction. The alpha-particle model[1] gives the same result. The observed width[23, 9] and mode of decay[24] of the state are also satisfied. Since gamma-ray de-excitation from 5/2 to 3/2 without change in parity must proceed by magnetic dipole radiation, the radiation width is of the order of 1 electron volt. Decay by neutron emission to the ground state of Be^8 requires the neutron to carry off three units of orbital angular momentum. A rough calculation for the probability of this process gives a partial width of about 1 kev.

D. Other Levels

Data have been presented which show that a level of Be^9 may exist at 1.8 Mev excitation. It has been pointed out, however, that the presence of peaks such as that shown in Fig. 10 may be a result of special effects which cause the three-body reaction $Be^9(x, nx')Be^8$ to preferentially emit near-maximum-energy charged particles x'. A more detailed discussion of this phenomenon is given in the next

subsection. Present numerical analysis of the intermediate-coupling shell model[3] favors 1/2 - for this state. If this were the case, the level would decay predominantly by neutron emission, with a lifetime of the order of 10^{-21} second. That is, the level width would be of the order of 1 Mev. The observed "level" fits such a prediction. Unfortunately, if the prediction is correct, conclusive proof of the existence of the level by detection of a 1.8-Mev gamma ray will be impossible.

The outstanding facts so far known about this "level" concern its formation. The cross section for formation by 12-Mev proton scattering in the angular interval $55^{\circ} < \theta < 97^{\circ}$ is only 100 microbarns/steradian. That is, its formation cross section is 1/75 that for the 2.43-Mev level. Its apparent absence in the inelastic alpha particle and deuteron measurements, indicates that the cross section for its formation in these reactions is at least as low as 1/2 millibarn/steradian. One must conclude either that the cross sections are near minima at all angles at which it was searched for or that the cross sections are simply small. On the other hand, in the reaction $Li^7(He^3, p)Be^{9*}$ the 2.43-Mev and the 1.8-Mev peaks are of comparable magnitude.[7] Unfortunately, absolute values were not determined in this work. It is impossible to say, therefore, whether the formation of the 1.8-Mev "level" is up, or whether the formation of the 2.43-Mev level is down. In any case it is clear that this "level" possesses properties different from the 2.43-Mev state.

If the 1.8-Mev "level" is a level, the anomaly would be explained if it does not arise from the p^5 configuration of the shell model. Since the ground state is a p^5 state, formation of the 1.8-Mev level from the ground state would then involve major changes in the nuclear structure.* On the other hand, its formation from Li^7 might proceed in a more direct manner. Information derived from other nuclei indicates, however, that the lowest p^4d or p^3d^2 states should not occur at excitation energies less that 5 or 10 Mev. If collective modes are excited in Be^9, the 1.8-Mev level could be one of these.

---

* Such changes are not encountered in the formation of the 2.43-Mev state, which also arises from the p^5 configuration.

The other possibility is that it is not a level at all. As is discussed in the next subsection, this interpretation is quite probable. Even in this case it may be still difficult to understand the variation in prominence of the 1.8-Mev peak.

Other previously reported levels of Be^9 at 3.1, 4.8, 6.8 and 11.3 Mev were also observed in these scattering experiments. Since the last two were definitely excited in inelastic alpha-particle scattering, their isotopic spin value 1/2 is established. Unfortunately, because of the high-level continuum beneath these peaks it was impossible to determine their formation cross sections. As pointed out above, the other levels (in alpha scattering) could have been masked by the continuum. Other work has shown that the 4.8-Mev level is broad--this breadth would have inhibited its observation in these experiments.

As for the 1.8-Mev "level," the cross sections for the formation of the 3.1- and 4.8-Mev levels by inelastic scattering are small compared with that for the 2.43-Mev state, while they are comparable in the $Li^7(He^3, p)Be^{9*}$ reaction.

It is interesting to conjecture that, just as the 1.8-Mev feature may be a pseudo level, the 4.8-Mev level may be also, owing to the same phenomenon. That is, 1.8 Mev bears the same relation to the Be^8 + n threshold (1.666 Mev) as 4.8 Mev does to the Be^{8*} + n threshold (4.6 Mev). In experiments to date the 4.8-Mev level has been found to have a width of about 1 Mev. The first excited state of Be^8 is as broad. If the 4.8-Mev level is a level and belongs to the p^5 configuration it is difficult to see how it could have such a width unless its spin were 1/2. There is only one low-lying J = 1/2 level in the p^5 configuration, and the best theory indicates that it should lie next to the 2.43-Mev level (i.e., the 1.8-Mev state or at least the 3.1-Mev state).

In summary, the peculiarities encountered among the low-lying levels of Be^9 are many. The most promising explanation is that these levels do not all arise from the p^5 configuration of the shell model. It is apparent that before a more satisfactory theory can be provided one must have a better idea of the types of levels involved. The spins and

parities of these levels must be determined; it would also be helpful to know more about the Li^9 beta transition. It goes without saying that it must be ascertained whether the 1.8- and 4.8-Mev levels are true or fictitious.

E. The Three-Body Reactions $Be^9(p, np')Be^8$ and $Be^9(\alpha, n\alpha')Be^8$

Prominent continua of protons and alpha particles were observed in this work. The maximum energy limits observed were in each case consistent with the interpretation noted. By the method outlined in the Appendix, cross sections were obtained for the reactions, in which more that 90% of the available energy is retained by the charged particle. These are shown in Figs. 14 and 18. The predominant forward peaking of these cross sections suggests that the reactions proceed by direct interaction. Two such processes are possible.

The reaction can be viewed as inelastic scattering in which the final state is not bound. Under these conditions, since the neutron can carry off any energy and any angular momentum, the scattered-particle distribution loses all structure. In other words, the spherical Bessel functions of the ABM theory are averaged over ℓ and k'. Since the zero-order Bessel function is dominant, a peak in the forward direction is to be expected. The experimental results verify this conclusion.

From another viewpoint the mechanism can be thought of as heavy-particle stripping.[52] To examine such a process in more detail, consider the specific case of the proton-induced reaction. In the center-of-mass frame before collision, the proton is traveling forward, the Be^9 nucleus backward. In analogy to deuteron stripping, heavy-particle stripping can occur if the Be^8 core collides with and is absorbed by the proton at a time when the neutron is outside the range of forces. The neutron will then be observed at an angle θ determined by the vector sum of its translational momentum and its instantaneous share of the internal momentum of Be^9. The outstanding difference between this

type of reaction and deuteron stripping is that the neutron distribution in the former will be peaked in the backward direction. Reaction cross sections of this type have been observed.[53] The positions of the maxima and minima determine the spin-parities involved in a manner similar to that in deuteron stripping.

In the above case, the Be^8 and proton were considered bound. If this does not happen, any angular momentum transfer and any energy loss for the proton are permitted. In a rough way the theory should be the same as that considered by Serber.[54] That is, the neutrons should be peaked in the backward direction and have an energy distribution symmetric about the value that they had because of the motion of the Be^9 in the center-of-mass frame. Detailed calculations of the effects of this momentum spread are now in progress. For consideration here, all that is needed is the fact that the most probable neutron momentum vector points backward along the beam axis and has a magnitude (in the center-of-mass system) given by

$$P'_n = \frac{M_n}{M_p + M_{Be^9}} \left(2 M_p E_p\right)^{1/2},$$

where the M's refer to the masses of the particles involved, and E_p is the laboratory-system energy of the incident proton. Once the neutron momentum vector is known, the three-body kinematics can be solved to yield an explicit expression for the scattered proton energy as a function of angle. This has been done and the expression evaluated for the angles at which the 1.8-Mev "level" was observed. It is then possible to transform these values into an effective Q value for levels in Be^9. These are compared below with the observed Q values of the 1.8 Mev "level."

Table X

A comparison of the observed Q values for the 1.8-Mev "level" and those which arise from unbound heavy-particle stripping

Angle (c.m.) (degrees)	Q_{obs} (Mev)	"Q" (calculated) (Mev)
55.4	- 1.76 ± .03	- 1.75
71.5	- 1.82 ± .03	- 1.80
97.0	- 1.91 ± .03	- 1.89

Not only does such an interpretation agree with the observed mean value for the Q, but it also reproduces the observed systematic shift with angle, a shift that is outside the expected errors of measurement. Until calculations on the effective "peak" width have been carried out it is impossible to say whether the characteristics of the "level" are completely reproduced by this model.

A third possibility for the reaction mechanism is compound-nucleus formation. Since such a process would undoubtedly yield a distribution symmetric about 90°, the (p, np') continuum offers conclusive evidence that direct interaction is appreciable at 12 Mev. The somewhat doubtful second interpretation of the 2.43-Mev inelastic proton-scattering data is consequently validated.

If the reaction were fundamentally a boil-off process, the distribution in energy of the charged particles would be given by the statistical phase-space expression[55]

$$N(E/E_{max}) \propto \left(\frac{E}{E_{max}}\right)^{1/2} \left(1 - \frac{E}{E_{max}}\right)^{1/2},$$

where E_{max} is determined by the kinematics of the reaction. By integration of this distribution it is possible to obtain the fraction of all the particles emitted that have an energy greater than 90% E_{max}.

Division of the observed differential cross sections by this number yields the total differential cross sections shown on the left of Figs. 14 and 18. Since direct-interaction processes can occur with the preferential emission of energetic charged particles, and since Coulomb effects would suppress low-energy charged-particle emission even if the compound nucleus were involved, these are upper limits only. The total integrated cross sections for these reactions are therefore $\sigma(p, np') < 185$ millibarns and $\sigma(\alpha, n\alpha') < 900$ millibarns. These values afford further proof that direct interaction is important here, since the geometric cross section of Be^9 is only ~ 300 millibarns.

F. Remarks About the Direct-Interaction Theories

In the preceding subsections various theories of direct interaction have been called upon to interpret experimental results so as to yield some of the properties of Be^9. Except where necessary for the interpretation, no remarks about the theories themselves and the interrelationship of their parameters have been made. Since a considerable body of data is now available for a single nucleus, some comments of this type are possible.

Three inelastic scattering processes have been investigated. Of these the 24-Mev deuteron theory fits its experiment best. Next in order of agreement with experiment comes the alpha-particle application of the ABM theory. Finally, it was found that the ABM theory is a poor fit for the 12-Mev proton data. Unfortunately the particles scattered were of different energies, so that it is difficult to assess separately the relative validity of the theories themselves and the energy regions in which they are most successful. However, if one considers the 31.3-Mev proton data as well, it might be inferred that for energies greater than, say, 20 Mev the theories are fairly accurate. Such a conclusion shows marked deviation from the results found for deuteron stripping. This direct-interaction theory is apparently adequate, at least down to energies as low as 8 or 10 Mev. Since the only major difference between deuteron stripping and inelastic scattering

is that a particle actually changes hands in the former, one might attach the greater success of the stripping theory to that exchange.

In all the direct-interaction theories the radius of interaction for best fit is considerably larger than the accepted nuclear radius. As was pointed out in earlier discussion, the larger values obtained are more logical when thought of as the sum of the nuclear radius and the particle radius. Further, since these reactions are presumed to proceed via interaction with the "tails" of the nuclear wave function, radii still larger than this sum might be expected.

The theory of the (d, p) reaction has seen widespread application to a large number of experimental results. Except in a few instances, reasonable fits have been obtained. In most of these exceptions, it has been possible to fit the data with the more accurate theories, including Coulomb interaction and nuclear scattering of the bystanding particle. There are few good opportunities to test the fit of the data for one reaction at a variety of energies. With the 12-Mev results presented here for $Be^9(p, d)Be^8$, data for this reaction are now available at bombarding energies of 5 to 8 Mev,[56] 12 Mev, 16.5 Mev,[57] 22 Mev,[58] and 31.3 Mev.[16] Figure 22 shows these data arbitrarily normalized for best fit. Apart from a slight tendency for the measured values to separate in the neighborhood of 70°, there is no evidence of any such energy variation in the shape as is predicted by the Butler theory.

It is hard to see how the revisions to the theory, that include Coulomb interaction, could lead to any improvement, since for $Z = 4$ such effects should be small. It is possible that nuclear interaction with the proton and deuteron is important. As observed by Bhatia et al.,[46] Butler's formula behaves in a "special" or "singular" manner when the neutron binding energy is zero. The Born approximation does not. Since the neutron binding energy is nearly zero for the reaction under consideration, it is possible that the theory is not valid in this case. Failing this explanation for the energy independence, one would have to conclude that special properties of beryllium are operative. Certainly no other such striking disagreement with the Butler theory has been observed.

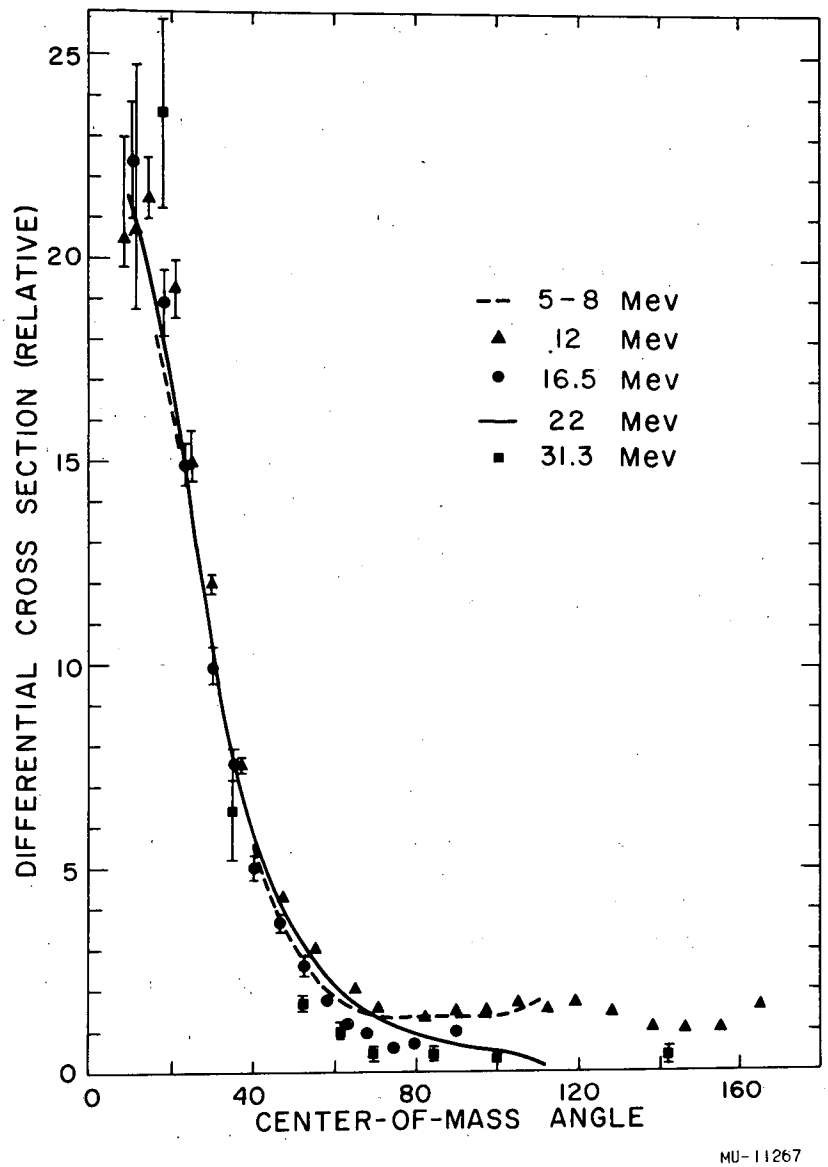

Fig. 22. The shape of the differential cross section for the reaction $Be^9(p, d)Be^8$ at various proton energies. The data were obtained from the references listed in the text.

As more and more experimental data for inelastic scattering reactions are obtained, the need for better theoretical calculations becomes more evident. In particular, it would be useful to estimate the interaction radii of the different particles. It is not even clear that such radii are energy-independent. In addition, it is time that rough indications of the absolute values of these fringe interactions were obtained. Of greatest importance among these would be quantitative estimates of the inelastic proton-scattering amplitudes with and without spin flip.

VI. CONCLUSIONS

Observations of the charged particles emitted from beryllium bombarded by 12-Mev protons, 24-Mev deuterons, and 48-Mev alpha particles have been carried out. From the analysis of these results, further properties of the direct-interaction theories and of the Be^9 nucleus have been derived. Most notable among the latter has been the assignment of the spin and parity (5/2 -) of the 2.43-Mev level. Evidence has been presented to discount the existence of a level in that nucleus at ~ 1.8 Mev.

ACKNOWLEDGMENTS

It is a pleasure to thank Professor A. C. Helmholz for his continued interest and advice in this work. The invaluable assistance of Drs. Robert E. Ellis, Franklin J. Vaughn, and Homer E. Conzett in setting up the cyclotron runs and taking data is gratefully acknowledged. The author is indebted to Professor David R. Inglis for several stimulating discussions. The late Mr. G. Bernard Rossi, Mr. W. B. Jones, and the other members of the 60-inch cyclotron staff provided excellent accelerator operation and frequently assisted beyond the call of duty. This work was greatly facilitated by Mr. Fred Vogelsberg, who maintained the counting area electronics.

The author would like to express appreciation for financial assistance received as Abraham Rosenberg Research Fellow (1953-54) and National Research Council of Canada Special Scholar (1954-56). This work was done under the auspices of the U. S. Atomic Energy Commission.

APPENDIX

It is common procedure to determine from a charged-particle spectrum the cross sections for reactions that yield discrete energy groups. By means of the analysis presented here, it is possible to obtain cross sections for multibody reactions that yield continuum spectra. In particular, it has been possible to measure the cross sections for the reactions $Be^9(p, np')Be^8$ and $Be^9(\alpha, n\alpha')Be^8$, in which the charged particle is emitted with 90% or more of the maximum energy permitted. For the sake of clarity, the particular case of the (p, np') reaction is discussed. Generalization is largely a matter of notation.

Consider the three-body breakup in the center-of-mass frame. Because the system has no net momentum, the momentum vectors $\vec{P}_n$, $\vec{P}_p$ and $\vec{P}_N$ ($\equiv \vec{P}_{Be^8}$) are necessarily coplanar. Choosing a coordinate system in this plane so that $\vec{P}_p$ is directed along the x-axis, we have the kinematical equations

$$P_p + P_n \cos \phi_n + P_N \cos \phi_N = 0,$$

$$P_n \sin \phi_n + P_N \sin \phi_N = 0,$$

$$\frac{P_p^2}{2m_p} + \frac{P_n^2}{2m_n} + \frac{P_N^2}{2m_N} = \mathcal{E},$$

where the angles are measured in the usual sense, the m's refer to the masses of the particles involved, and $\mathcal{E}$ is the energy of the system. The maximum value of P_p (and hence of the proton energy E_p) is obtained when $\phi_n = \phi_N = 180^\circ$ and $P_n/m_n = P_N/m_N$. It is an easy matter to establish that

$$(E_p)_{max} = \frac{(P_p)^2_{max}}{2m_p} = \frac{m_n + m_N}{m_p + m_n + m_N} \mathcal{E}.$$

It is useful to express the actual energy* of the emitted proton as a fraction of this maximum energy. Thus we define $x = E_p/(E_p)_{max}$.

Preparatory to transforming to the laboratory frame, consider now that the proton momentum is actually at angle θ with respect to some space-preferred direction (i.e., the direction of incidence of the initial proton). Equations for the angles and energies of the neutron and nucleus are now extremely cumbersome (azimuthal symmetry has been lost). These do not concern us, however. When we put in the features of the initial collision and transform to the laboratory system, it is easy to show that

$$\mathcal{E} = E_i \left[1 - \frac{m_p}{m_p + m_n + m_N} \right] + Q$$

and

$$A \left(\frac{E_f}{E_i} \right)^{1/2} = \cos \theta_L + \left\{ \cos^2 \theta_L + B \right\}^{1/2},$$

where

$$A = \frac{m_n + m_p + m_N}{m_p},$$

---

* When the proton does not take maximum energy, the neutron and the Be^8 nucleus are allowed to have various energies and angles. They do not have complete freedom, however, until x is sufficiently small. In particular the angles are confined to the solid cones given by

$$\cos \phi_n \leq -\left[\frac{m_n + m_N}{m_p \; m_n} \left\{ m_p + m_N \; x - \frac{m_N(m_p + m_n + m_N)}{m_n + m_N} \right\} \right]^{1/2}$$

and

$$\cos \phi_N \leq -\left[\frac{m_n + m_N}{m_p \; m_N} \left\{ m_p + m_n \; x - \frac{m_n(m_p + m_n + m_N)}{m_n + m_N} \right\} \right]^{1/2}.$$

As a consequence, when the proton takes near maximum energy, the other two particles are closely confined in a small-angle cone and travel with nearly equal velocity. It is this fact which has prompted the hypothesis that the 1.8-Mev "level" (which would correspond to near-maximum proton energy if the three-body process were involved) may arise from resonance interaction between the unbound neutron-Be^8 system.

$$B = \left(\frac{m_n + m_p + m_N}{m_p}\right)^2 \frac{E_p}{E_i} - 1,$$

E_i = laboratory energy of the incident proton,

E_f = laboratory energy of the final proton,

Q = energy release in the reaction = -1.666 Mev,

and θ_L = laboratory angle of observation of the final proton corresponding to θ in the center-of-mass system.

With the equations above it is possible to determine, for any laboratory angle θ_L, the laboratory energies corresponding to any desired center-of-mass proton energies.

In order to obtain a meaningful result for the relative differential cross section of such a reaction, it is necessary to take measurements at various angles of the number of scattered protons within some constant center-of-mass energy interval. The interval chosen in this investigation was $0.90\,(E_p)_{max} \leq E_p \leq (E_p)_{max}$. After calculation of the equivalent laboratory energies, and of their equivalent ranges, it was possible to identify the corresponding interval of the observed proton spectra. As an example, these limits are shown by the arrows R_H and R_L in Fig. 9 for $\theta_L = 21^\circ$. Since the 2.43-Mev inelastic peak and the pickup deuterons are superimposed on the continuum in this region, it was necessary to interpolate between the end point and a region where nothing interfered with the observation of the continuum alone. These interpolations were done linearly for simplicity.*

---

* The combination of the statistical center-of-mass energy distribution, the range-energy distortion, and the effect of converting to the laboratory frame results in a shape that deviates far from linearity at the end point. Since it was expected that the statistical assumption would be wrong, linear interpolation was tried. The differential cross section obtained shows the validity of the expectation. The symmetry of the peaks obtained by subtraction of a linear continuum proves that linear interpolation is not seriously in error.

From the area of the triangle of continuum so defined and the counter range bite, an X was calculated. The remainder of the calculations follow in the same way as those for a peak. No corrections were applied for the finite energy resolution of the counter. Since the continuum shape is not a rapid function of range, it seems justifiable to think that on the average the number of particles lost from the interval was equal to the number gained. The transformation from laboratory to center-of-mass system was carried out by using the $G = \frac{d\Omega_L}{d\Omega}$ and the θ_L to θ correspondence for the median proton energy $0.95\ (E_p)_{max}$.

REFERENCES

1. R. R. Haefner, Revs. Modern Phys. 23, 228 (1951).
2. M. G. Mayer, Phys. Rev. 75, 1969 (1949).
3. French, Halbert, and Pandya, Phys. Rev. 99, 1387 (1955); D. Kurath, Phys. Rev. 101, 216 (1956); D. R. Inglis, Revs. Modern Phys. 25, 390 (1953).
4. J. S. Blair and E. M. Henley, Bull. Am. Phys. Soc. 1, 20 (1956).
5. F. Ajzenberg and T. Lauritsen, Revs. Modern Phys. 27, 77 (1955).
6. E. Guth and C. J. Mullin, Phys. Rev. 76, 234 (1949).
7. Moak, Good, and Kunz, Phys. Rev. 96, 1363 (1954).
8. L. L. Lee, Jr. and D. R. Inglis, Phys. Rev. 99, 96 (1955).
9. Gossett, Phillips, Schiffer, and Windham, Phys. Rev. 100, 203 (1955).
10. Rasmussen, Miller, Sampson, and Gupta, Phys. Rev. 100, 851 (1955).
11. Marion, Bonner, and Cook, Phys. Rev. 100, 91 (1955); F. Ajzenberg and W. W. Buechner, Phys. Rev. 91, 674 (1953).
12. McIntyre, Hahn and Hofstadter, Phys. Rev. 94, 1084 (1954).
13. K. E. Davis, Phys. Rev. 88, 1433 (1952).
14. H. F. Stoddart, MIT Progress Report, May 1953 (unpublished).
15. R. Britten, Phys. Rev. 88, 283 (1952).
16. R. G. Finke, Charged Particles from Beryllium Bombarded by 31.3-Mev Protons (Thesis), UCRL-2789, Nov. 1954; Benveniste, Finke, and Martinelli, Phys. Rev. 101, 655 (1956).
17. J. N. McGruer, (private communication to F. Ajzenberg and T. Lauritsen).
18. W. O. McMinn, M. B. Sampson, and V. K. Rasmussen, Phys. Rev. 84, 963 (1951).
19. D. M. Van Patter, A. Sperduto, K. Huang, E. N. Strait, and W. W. Buechner, Phys. Rev. 81, 233 (1951).
20. F. L. Ribe and J. D. Seagrave, Phys. Rev. 94, 934 (1954).
21. K. W. Allen, (private communication to F. Ajzenberg and T. Lauritsen).
22. K. W. Allen and E. Almqvist, (private communication to F. Ajzenberg and T. Lauritsen).

23. Browne, Williamson, Craig, and Donahue, Phys. Rev. 83, 179 (1951).

24. G. A. Dissanaike and J. O. Newton, Proc. Phys. Soc. (London) 65A, 675 (1952).

25. S. T. Butler, Proc. Roy. Soc. (London) A208, 559 (1951).

26. Austern, Butler, and McManus, Phys. Rev. 92, 350 (1953).

27. Gardner, Knable, and Moyer, Phys. Rev. 83, 1054 (1951); R. K. Sheline, Phys. Rev. 87, 557 (1952); W. F. Fry, Phys. Rev. 89, 325 (1953).

28. L. M. Baggett and S. J. Bame, Jr., Phys. Rev. 85, 434 (1952).

29. R. Nathans and J. Halpern, Phys. Rev. 92, 940 (1953).

30. Haslam, Katz, Crosby, Summers-Gill, and Cameron, Can. J. Phys. 31, 210 (1953).

31. G. E. Fischer, The Scattering of 10-Mev Protons on Carbon and Magnesium (Thesis), UCRL-2546, April 1954; G. E. Fischer, Phys. Rev. 96, 704 (1954).

32. R. E. Ellis, Elastic Scattering of 48-Mev Alpha Particles by Heavy Nuclei (Thesis), UCRL-3114, Aug. 1955.

33. F. J. Vaughn, Elastic and Inelastic Scattering of 48-Mev Alpha Particle by Carbon and Magnesium, UCRL-3174, Oct. 1955.

34. W. F. Hornyak and R. Sherr, Phys. Rev. 100, 1409 (1955).

35. B. Rossi, "High-Energy Particles," N. Y., Prentice-Hall, 1952, p. 29 ff.

36. Fulbright, Bruner, Bromley, and Goldman, Phys. Rev. 88, 700 (1952); F. A. El-Bedewi, Proc. Phys. Soc. (London) 64A, 947 (1951).

37. Eisberg, Igo, and Wegner, Phys. Rev. 99, 1606 (1955).

38. Bashkin, Petree, Mooring, and Peterson, Phys. Rev. 77, 748 (1950).

39. J. M. Blatt and V. F. Weisskopf, "Theoretical Nuclear Physics," N. Y., Wiley, 1952, p. 357.

40. Igo, Wegner, and Eisberg, Phys. Rev. 101, 1508 (1956).

41. E. Segrè, (editor), "Experimental Nuclear Physics," Vol. 1, N. Y., Wiley, 1953, part IV and page 477 in particular.
42. R. D. Woods and D. S. Saxon, Phys. Rev. 95, 577 (1954).
43. Melkanoff, Moszkowski, Nodvik, and Saxon, Phys. Rev. 101, 507 (1956); Melkanoff, Nodvik, Saxon, and Woods, Technical Report No. 7-12-55, Dept. of Physics, UCLA., 1955.
44. Shaw, Conzett, Slobodrian, and Summers-Gill, Bull. Am. Phys. Soc., to be published.
45. R. G. Thomas, Phys. Rev. 100, 25 (1955). This article gives an excellent list of references to other theoretical studies.
46. Bhatia, Huang, Huby, and Newns, Phil. Mag. 43, 485 (1952).
47. R. Huby and H. C. Newns, Phil. Mag. 42, 1442 (1951).
48. J. R. Holt and C. T. Young, Nature 164, 1000 (1949); Freemantle, Gibson, and Rotblat, Phil. Mag. 45, 1200 (1954).
49. G. R. Satchler, Proc. Phys. Soc. (London) 68A, 1037 (1955).
50. H. E. Conzett (private communication).
51. For example, see J. M. Blatt and V. F. Weisskopf, "Theoretical Nuclear Physics," N. Y., Wiley, 1952, p. 535 ff.
52. L. Madansky and G. E. Owen, Phys. Rev. 99, 1608 (1955).
53. Risser, Class, and Price, Bull. Am. Phys. Soc. 1, 20 (1956).
54. For example, see O. R. Frisch, (editor), "Progress in Nuclear Physics," Vol. 3, N. Y., Academic Press, 1953, Article 7.
55. G. E. Uhlenbeck and S. Goudsmit, "Pieter Zeeman 1865-25 Mei-1935," The Hague, Martinus Nijhoff, 1935, p. 201 ff.
56. J. A. Harvey, MIT Progress Report NP-3434, Oct. 1950, p. 58.
57. J. B. Reynolds and K. G. Standing, Phys. Rev. 101, 158 (1956).
58. Cohen, Newman, Handley, and Timnick, Phys. Rev. 90, 323 (1953).